

CHAPTER 1

PHYSIOLOGICAL INTRODUCTION

The overall arrangement of the mammalian cardiovascular system can be summarised briefly as follows. The heart is composed of four chambers arranged in two pairs. The thin-walled atrium on each side is connected through a valved orifice to a thick-walled muscular ventricle; each ventricle connects in turn to a major distributing artery, the mouth of which is again guarded by a valve. The left ventricle is the thicker and leads to the aorta (diameter about 2.5 cm in man), through which oxygenated blood is distributed to the tissues of the body. Large arteries branch off the aorta, smaller ones branch off them, and so on for many subdivisions; the number of branchings along any pathway depends on the particular organ being supplied. The final subdivisions of the arterial tree are the arterioles, which have very muscular walls and internal diameters in the range 30–100 μm . These vessels give rise to the capillaries (diameters down to 4 or 5 μm) across the walls of which the principal exchange of fluids and metabolites between blood and the tissues takes place. The blood passes from the capillaries into the smallest veins (venules) and thence into a converging system of increasingly larger veins, finally merging into the superior and inferior venae cavae which join directly to the right atrium of the heart. (An exception to this pattern is the circulation in the heart muscle itself, which drains directly into the right atrium.) From the right atrium, blood is transferred to the right ventricle, and thence to the pulmonary artery, which leads through a bifurcating system of arteries to the pulmonary capillaries in the walls of the alveoli of the lung, where gas exchange takes place. From there the re-oxygenated blood is returned to the left atrium via the pulmonary veins, and the cycle is repeated. The average time taken for an element of blood to complete one circuit of the system is about one minute (in man).

The aim of this book is to explain the physical processes involved in the circulation of the blood in the large vessels of the circulation. The microcirculation (arterioles, capillaries and venules) is excluded for the reasons given in the preface; it is convenient that the conventional definition of the microcirculation, as consisting of all vessels which cannot be seen except through a microscope (i.e. of diameter less than about 100 μm), conforms closely to a definition more appropriate from the fluid mechanical point of view, namely vessels in which the mean Reynolds number is normally less than 1. Thus we shall be concerned with aspects of the circulation for which fluid inertia is important, and, as it turns out, for which blood can be considered a homogeneous Newtonian fluid (see § 1.2). This chapter is intended to set the scene by describing both the physical properties of the system and the phenomena which it is physiologically important to analyse. We also consider the fluid mechanics of the left ventricle in § 1.3.

Many books and reviews have already been published on the fluid mechanics of the circulation. Among the most important, on which I have leaned heavily for the material of this chapter and the next, are the two editions of *Blood Flow in Arteries* by McDonald (1960, 1974), the two-volume work edited by Bergel (1972*a*), Bergel & Schultz (1971), chapters 12 and 13 of Lighthill (1975) and the proceedings of various symposia (Attinger, 1964; ASME, 1966; Fung, 1966; Fung, Perrone & Anliker, 1972). Considerable detail on the structure and properties of the whole cardiovascular system, together with much physical (but not mathematical) discussion of the fluid mechanics, is given in a book of which I am a joint author (Caro *et al.*, 1978); most of the information in § 1.1 of this monograph is also contained in that work.

1.1 Anatomy, wall structure and mechanical properties

While the principal aim of the study of cardiovascular mechanics is to understand the circulation in man, most experimental data have been obtained in other mammals, especially dogs. Where the difference is important in what follows, it is mentioned; usually, however, the fluid mechanics is not well enough understood for

small inter-species differences to be important except in the matter of scale. Most of the quantitative values to be given will apply to the dog.

1.1.1 *The heart*

The two atria are comparable in structure, and are separated from each other by a common wall, the inter-atrial septum. The veins drain into them without valves. The atrio-ventricular valve on the right side has three cusps (or flaps) while that on the left (the mitral valve) has only two. In each case the edges of the cusps are tethered to the opposite wall of the ventricle by fine cords anchored in small slips of muscle (papillary muscle). These cords have no active function in the opening or closing of the valves, which occur passively (see § 1.3), except to prevent the valves turning inside out and allowing backflow when they have closed. The exit valves from the ventricles (the pulmonary and aortic valves) are similar to each other, each consisting of three cusps that can open to the full cross-section of the artery without coming into contact with the artery wall, because behind each cusp is an outpouching of the artery, or sinus. In the aorta these sinuses are called the sinuses of Valsalva; the coronary arteries branch off two of them. The sinuses have an important function in the operation of the valve, as discussed in § 1.3.

The four valve orifices in the heart are aligned approximately in the same plane (fig. 1.1), and the cusps of each are attached at their bases to a stiff ring of fibrous tissue. The four rings are in turn connected to each other by fibrous tissues, so that the valve plane forms a stiff framework to which the muscles of all the chambers are attached, as are the origins of the pulmonary artery and the aorta. The heart as a whole is slung in a thin but inelastic fibrous bag, the pericardium, which in turn is attached to other structures within the chest, including the spine. The stress-strain relation of the pericardium is, like all fibrous tissues consisting largely of collagen, highly non-linear. Under normal conditions the pericardium is relatively unstretched, and has little effect on pressures and volumes in the heart; in certain diseases, however, fluid accumulates in the pericardium, which becomes taut and constrains the maximum volume of the heart.

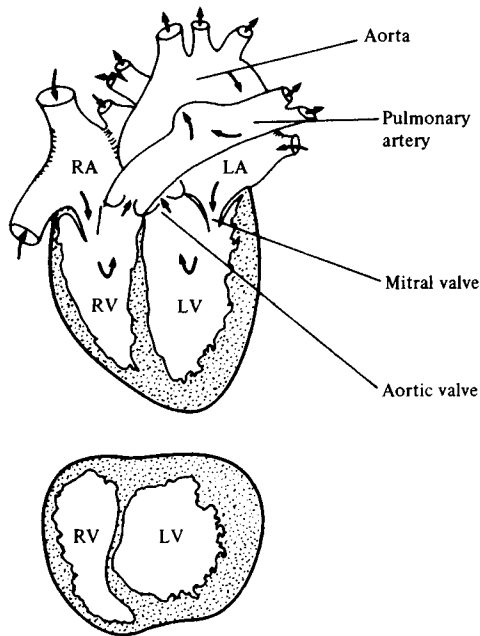


Fig. 1.1. Schematic diagram of a longitudinal and a horizontal cross-section of the heart, showing inflow and outflow tracts and valvular arrangement. Note the differences in the shape of the cross-sections and in the wall thicknesses of the two ventricles. RV, right ventricle; LV, left ventricle; RA, right atrium; LA, left atrium. (After Attinger, 1964.)

The left ventricle is shaped rather like a blunted arrowhead with the valves at its base (fig. 1.1), and with a roughly circular transverse cross-section. When the ventricle contracts, but before the aortic valve opens, the long axis first shortens slightly while the transverse cross-section expands so that the included volume remains constant. However, when ejection begins, the long axis shortens only very little, while the transverse axes shorten by about a third: by the end of systole (the ejection phase) the ratio of long to short axes is about 2.5 to 1, having been about 1.5 to 1 in diastole (the resting phase). A reasonable model of left ventricular shape, for the purposes of fluid mechanical calculations, is that of a prolate spheroid, whose major axis remains constant during ejection, but whose minor axes contract significantly. The two valves would both be at one end of the spheroid. This model involves considerable

approximation, but the inaccuracy of measurement of ventricular dimensions *in vivo* is so great that the approximation is not unjustified. The end-diastolic volume of the left ventricle in a 20-kg dog is about 40 cm^3 , and about 20 cm^3 is ejected each beat (the corresponding figures in man are 140 cm^3 and 70 cm^3).

The right ventricle has been studied far less thoroughly than the left, but it is known to behave very differently. One wall is functionally part of the left ventricular wall, while the other, free wall is much thinner and has a larger area, so that the cavity of the right ventricle is wrapped round one side of the left ventricle like a pocket, opening at the top into the pulmonary artery and right atrium (fig. 1.1). The operation of the right ventricle is like that of a check-valve pump (Carlsson, 1969): during systole the free wall moves downwards, carrying the open pulmonary valve past the blood in the ventricle; during diastole it moves up again, the closed valve pushing the blood up with it. It is clear from continuity considerations that the amount of blood ejected each beat by the right ventricle must, on average, be the same as that ejected by the left.

The walls of the chambers of the heart consist almost entirely of muscle fibres, interspersed with collagen. Cardiac muscle is a form of striated muscle, as is skeletal muscle, but it differs in its electrical and mechanical properties. For instance, continuous stimulation of skeletal muscle held at a fixed length produces a sustained contraction (or tetanus) with a highly reproducible tension; this is the maximum tension that can be generated by that muscle at that length. Continuous stimulation of cardiac muscle, however, does not produce a tetanus, because the muscle repolarises slowly, so experiments to investigate its intrinsic contractile properties have to be much more elaborate (for example, a series of individual 'twitches' is commonly generated). Further, Hill (1938) showed experimentally that when tetanised skeletal muscle fibres contract against a constant force F , then (a) the rate of heat production is proportional to the speed of shortening V (i.e. equal to aV , say, where a is a constant), and (b) the total rate of energy production is linearly related to F , i.e.

$$(F + a)V = b(F_0 - F), \quad (1.1)$$

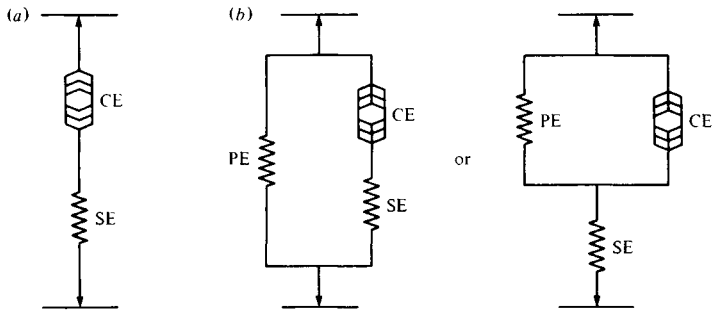


Fig. 1.2. Models of skeletal muscle. (a) A contractile element (CE) and an elastic element in series (SE); there is no tension when CE is relaxed. (b) Two possible arrangements in which a parallel elastic element (PE) supplies a 'resting tension'.

where b and F_0 are also constants. These results were obtained when the length of the muscle fibre at the start of the contraction was short enough for the 'resting tension' to be negligible, in which case a muscle fibre can be modelled as a 'contractile element' in series with a 'series elastic element' (fig. 1.2(a)). At greater lengths there is an initial tension in unstimulated muscle. This has to be accounted for by incorporating a 'parallel elastic element' into the model (fig. 1.2(b)), and by permitting a , b , F_0 in (1.1) to be functions of length, L .

No simple equation like (1.1) is applicable to heart muscle, however. This is partly because heart muscle cannot be tetanised, partly because individual muscle fibres cannot be separated as easily as in skeletal muscle, so the experiments are performed on small strips of (cat) papillary muscle in which some muscle fibres may not be parallel to the sides of the strip, and partly because at all lengths from which contraction is possible there is a significant resting tension. The absence of a tetanised state means that the time from the beginning of a twitch is an important variable in any relation between length, tension and velocity for cardiac muscle fibres, and no single model has been generally agreed. Fung (1970) has proposed the following equation, which can accommodate general non-linear and viscoelastic 'elastic elements':

$$\frac{d\Delta}{dt}(S, \Delta, t) = \frac{\pm b(\Delta)}{a(\Delta) + S} \left| \left[S_0(\Delta) \lambda \sin \frac{\pi(t+t_0)}{2t_m} - S \right] \right|^n. \quad (1.2)$$

In this equation Δ is the length of overlap between the actin and myosin filaments in the muscle sarcomere (a more fundamental measure of contractile element state than fibre length L), S is the stress in the series element, $S_0(\Delta)$ is the maximum attainable isometric tensile stress at overlap length Δ , n is an exponent whose value lies between 0 and 1 (in many cases being in the range 0.5–0.6), t_0 is a phase shift signifying the sudden initiation of active state at the time of stimulation, $2t_m$ is the time to peak activity, λ is an amplitude factor, $a(\Delta)$, $b(\Delta)$ are variable functions corresponding to a and b in (1.1), and the $+$ or $-$ is chosen according to whether the quantity in the square brackets in (1.2) is positive (stretching) or negative (relaxing). Equation (1.2) has the capacity to describe virtually all experimental results, but detailed testing of it, and empirical or theoretical evaluation of the functions and constants involved, are far from complete. Progress is necessarily piecemeal; for example, Brutsaert & Sonnenblick (1969) have shown that S_0 varies approximately linearly with length over a wide range of lengths:

$$S_0 = k_1 L + k_2, \quad (1.3)$$

where k_1 and k_2 are physiological constants.

A major practical difficulty with using (1.2) is the fact that most of the experiments on papillary muscle preparations have ignored two important factors: (a) the ends of the strips of muscle are inevitably damaged when clamped in the apparatus (Krueger & Pollack, 1975), and (b) even if they are not damaged, the strain in the middle section of a strip will differ from that at the constrained ends; this was demonstrated theoretically from finite-deformation elasticity theory by Hunter (1975). All the experiments therefore need to be repeated. Thorough reviews of the state of knowledge of heart muscle mechanics are given by Blinks & Jewell (1972) and by Caro *et al.* (1978, chapter 11).

Even if a model of the behaviour of heart muscle fibres were generally accepted, applying it to describe the mechanical behaviour of the intact heart would be extremely difficult. This is because of the intricate way in which the muscle fibres are arranged within the heart wall. The left ventricle is the only chamber whose

wall structure has been examined systematically. In it there is a continuous distribution of fibre orientation across the wall thickness. The innermost fibres run predominantly longitudinally from the stiff region round the valves (the base) to the other end of the chamber (the apex), which is an elongated cavity with roughly circular cross-section. The next layer of fibres is at a slight angle to the axis of the chamber, so that the fibres form a slight spiral. The angulation of the spiral increases in successively deeper layers, so that approximately half-way through the wall the fibres run circumferentially round the small cross-sections of the chamber. Thereafter the angulation continues, so that the outermost fibres are again longitudinal. Streeter *et al.* (1970), who described this arrangement, also used it as the basis for a prediction of normal and tangential stresses throughout the wall, on the assumption that each muscle fibre exerts the same tension. Predictions were made both for diastole, when the muscle is relaxed, and for systole, when it is contracted. In each case the tangential (hoop) stress is predicted to be greatest in the middle layers of the wall, with a slight bias to the outer surface in systole, while the normal stress is predicted to be greatest on the surface, especially on the inner surface during systole (when the pressure in the ventricle exceeds that outside by about 16 kN m^{-2} , or 120 mmHg). It would be possible to use an equation like (1.3) in Streeter *et al.*'s model, in order to incorporate more details of muscle behaviour, especially during contraction, but without more information on the resting lengths and tensions of the individual fibres, such predictions would be almost worthless. Without them, however, there is no link between the mechanics of individual muscles and that of the intact ventricle, and the latter must be described empirically.

Note that it is important to know something of the stress distribution in the ventricle wall, because the blood supply to the heart muscle is carried in coronary arteries which are embedded in it, and are therefore squeezed when the muscle contracts. Since coronary artery disease is one of the major causes of death in Western society, all information on coronary artery mechanics has potential clinical importance.

From the point of view of the rest of the circulation, contraction of the left ventricle produces a certain flow-rate into the aorta, Q_a ,

and a pressure, p_a , at its entrance. Thus an index of the effectiveness of the ventricle can, in principle, be obtained by measuring these quantities. However, no satisfactory index of 'cardiac contractility' has yet been proposed, because the chain of events linking muscle performance to aortic pressure and flow-rate has not been fully described. In § 1.3 we analyse a small link in that chain by examining the relation between aortic pressure and flow-rate (relatively easy to measure *in vivo*) and the mean pressure exerted by the ventricular muscle, p_v , together with ventricular volume, V . The former can be related to the average tension in the ventricle wall, and hence to Streeter *et al.*'s model, as long as both V and the shape of the ventricle, as it contracts, are known. However, no accurate way of measuring V is available, and only qualitative observations of the shape have been made, as described above. Quantitative details of the time variation of ventricular and aortic pressures, and of aortic flow-rate, are given in § 1.2.

1.1.2 *The systemic arteries*

The anatomy of the canine aorta and its main branches is illustrated in fig. 1.3, and many of the relevant dimensions are listed in table 1.1 (which was first published in Caro, Pedley & Seed (1974)). The initial part of the aorta, after the sinuses of Valsalva, is relatively straight for about 3 cm and is called the ascending aorta. The aorta then curves, in a complicated three-dimensional way, through about 180° (the 'arch'), giving off two branches to the head and upper limbs (there are normally three branches in man). It then pursues a fairly straight course down through the diaphragm (giving off nine pairs of small intercostal arteries) to the abdomen, where it distributes branches to the abdominal organs. Low down in the abdomen it terminates, forming two iliac arteries and the sacral artery (absent in man). All other large arteries, similarly, are curved and branched in a complicated way; there are relatively few straight segments of artery without branches where the fluid mechanics of long straight tubes can be applied, and more general theories are usually required.

The aorta (like most other arteries) tapers along its length. The rate of taper appears to be quite variable from animal to animal and, presumably, from species to species; however, in the dog, the area

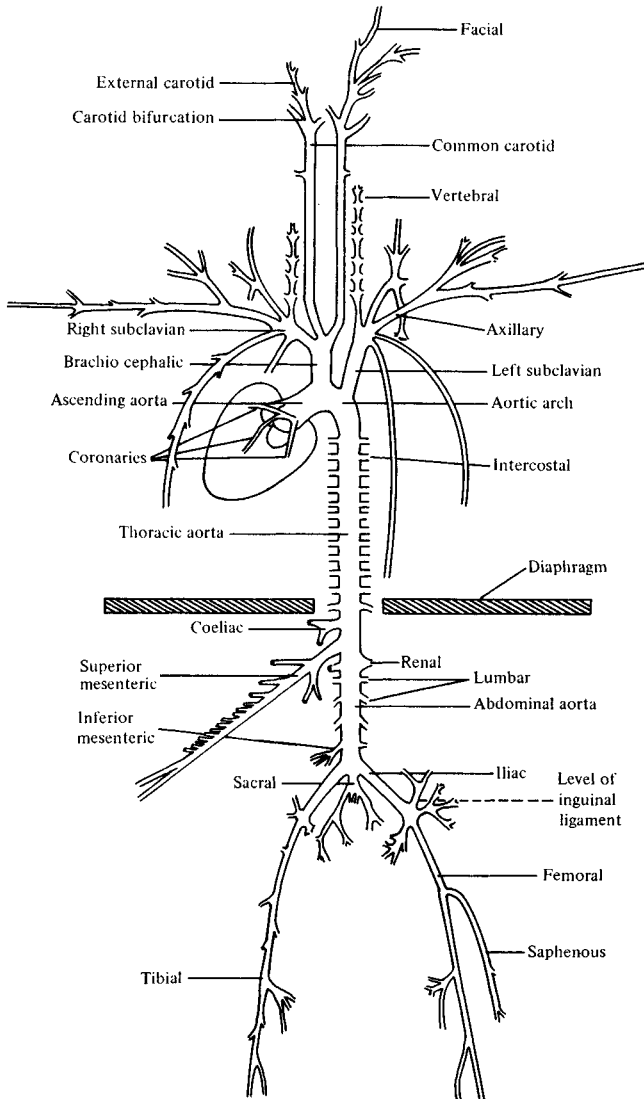


Fig. 1.3. A diagrammatic representation of the major branches of the canine arterial tree. (After McDonald, 1974.)

Table 1.1. Normal values for canine cardiovascular parameters. An approximate average value, and then the range, is given where possible. All values are for the dog except those for arteriole, capillary, and venule, which have only been measured in smaller mammals

Site	Ascending aorta	Descending aorta	Abdominal aorta	Femoral artery	Carotid artery	Arteriole	Capillary	Venule	Inferior vena cava	Main pulmonary artery
Internal diameter, d_i (cm)	1.5 1.0–2.4	1.3 0.8–1.8	0.9 0.5–1.2	0.4 0.2–0.8	0.5 0.2–0.8	0.005 0.001–0.008	0.0006 0.0004–0.0008	0.004 0.001–0.0075	1.0 0.6–1.5	1.7 1.0–2.0
Wall thickness, h (cm)	0.065 0.05–0.08		0.05 0.04–0.06	0.04 0.02–0.06	0.03 0.02–0.04	0.002	0.0001	0.0002	0.015 0.01–0.02	0.02 0.01–0.03
h/d_i	0.07 0.055–0.084		0.06 0.04–0.09	0.07 0.055–0.11	0.08 0.053–0.095	0.4	0.17	0.05	0.015	0.01
In-vivo length (cm)	5	20	15	10	15 10–20	0.15 0.1–0.2	0.06 0.02–0.1	0.15 0.1–0.2	30 20–40	3.5 3–4
Approximate cross- sectional area (cm ²)	2	1.3	0.6	0.2	0.2	2×10^{-5}	3×10^{-7}	2×10^{-5}	0.8	2.3
Total vascular cross- sectional area at each level (cm ²)	2	2	2	3	3	125	600	570	3.0	2.3
Peak blood vel- ocity (m s ⁻¹)	1.2 0.4–2.9	1.05 0.25–2.5	0.55 0.5–0.6	1.0 1.0–1.2		0.75	0.07	0.35	0.25 0.15–0.4	0.7
Mean blood vel- ocity (m s ⁻¹)	0.2 0.1–0.4	0.2 0.1–0.4	0.15 0.08–0.2	0.1 0.1–0.15		0.005–0.01	0.0002–0.0017	0.002–0.005		0.15 0.06–0.28
Peak Reynolds number, Re	4500	3400	1250	1000		0.09	0.001	0.035	700	3000
Frequency parameter, α (heart-rate 2 Hz)	13.2	11.5	8	3.5	4.4	0.04	0.005	0.035	8.8	15
Calculated wave speed, c_0 (m s ⁻¹)	5.8		7.7	8.4	8.5				1.0	3.5
Measured wave speed, c (m s ⁻¹)	5.0 4.0–6.0		7.0 6.0–7.5	9.0 8.0–10.3	8.0 6.0–11.0				4.0 1.0–7.0	2.5 2.0–3.3
Young's modulus, $E (\times 10^2 \text{ kN m}^{-2})$	4.8 3–7		10 9–11	10 9–12	9 7–11				0.7 0.4–1.0	6 2–10

change fits quite well to an equation of the form

$$A = A_0 e^{-\beta x/a_0}, \quad (1.4)$$

where A is aortic area, A_0 and a_0 are the area and radius at a given upstream site, x is the distance from that site, and β is a dimensionless number lying between 0.02 and 0.05. In man the taper is not as smooth as implied by (1.4).

Although arteries taper individually, the total cross-sectional area of the arterial tree increases with distance from the heart, because at most bifurcations the ratio of the summed areas of the two daughter tubes to that of the parent is greater than 1. However, accurate measurements of this area ratio at individual bifurcations *in vivo* are hard to obtain, and measurements in dead animals may not be valid if the arteries are not inflated to physiological pressures, or if they are dissected out of the animal before being measured. Our knowledge is therefore incomplete; the most reliable information concerns the aorta of a dog, as measured by Patel *et al.* (1963*b*) and shown in fig. 1.4. The values of the area ratio, as defined above, range from 0.79 to 1.29. The branches within the chest have ratios close to 1.0, while those in the upper abdomen have slightly higher values, but there is a marked contraction (ratio 0.85–0.90) at the termination of the aorta, which is also found in man (Caro, Fitzgerald & Schroter, 1971). It is downstream from the aorta that the area begins to increase sharply.

The angles at which branches come off the aorta and other arteries vary considerably, although most angles off the aorta are closer to 90° than to 0° or 180°; further downstream, smaller branching angles are more common. Most branches can be seen from fig. 1.3 to be asymmetrical; indeed, there are no symmetrical bifurcations in the dog, while in man the only example is the aortic bifurcation.

The coronary arteries (fig. 1.5(*a*)) form a special group both because of their importance in disease and because they are arranged slightly differently. The first branches off the left coronary artery are depicted in fig. 1.5(*b*). The first bifurcation, where the left common coronary artery divides into the left circumflex and left anterior descending arteries, is roughly symmetrical with a branch angle of about 45°, but it is unusual in that the whole junction is set

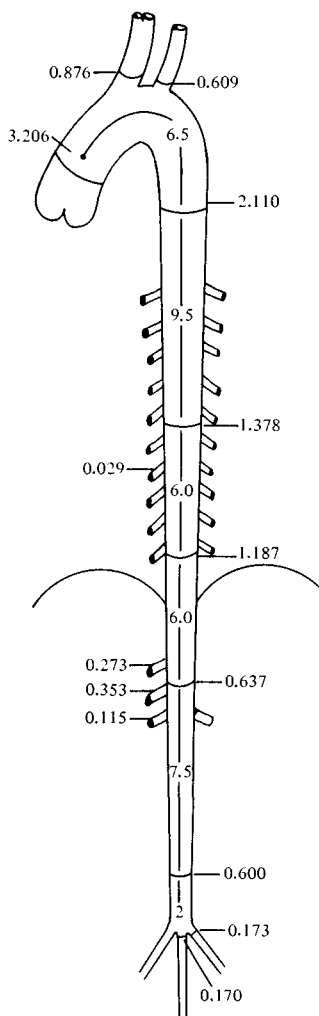


Fig. 1.4. Internal cross-sectional areas (cm^2) at various sites in the canine aorta and its main branches. (After Patel *et al.*, 1963*b*.)

out on a curved surface, the outside of the heart. Further downstream, both arteries and their branches become increasingly embedded in the heart muscle, with important consequences for their elastic properties.

The walls of all arteries (and veins) have a similar structure and are made up of similar materials, although their proportions vary in

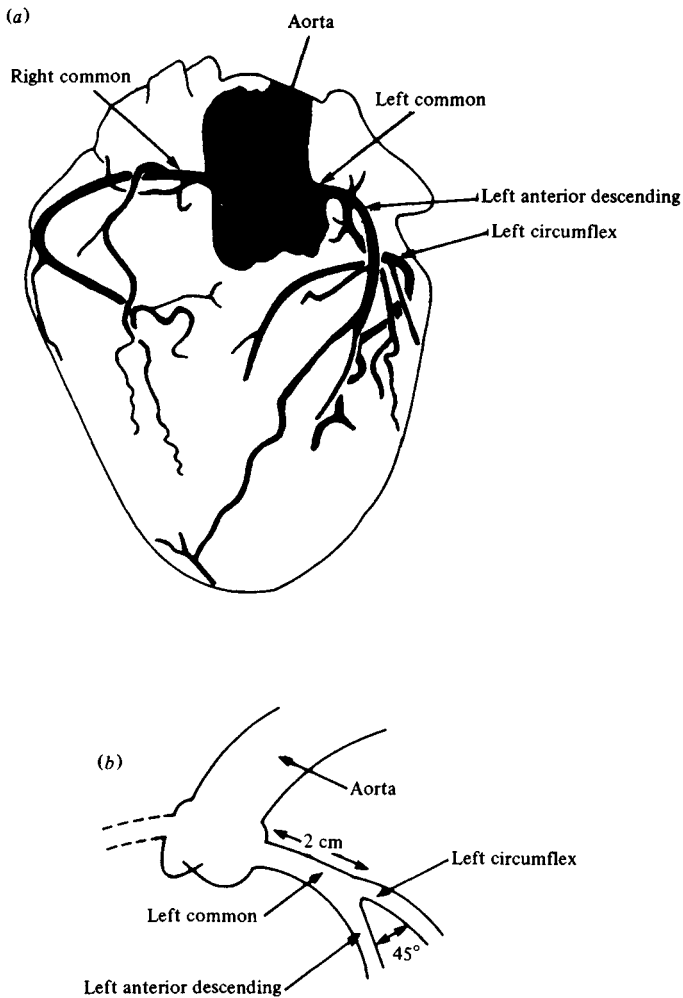


Fig. 1.5. (a) Diagram of the coronary arterial system (after Lusza, 1974), with (b) a schematic diagram of the major arteries on the left side of the heart.

different parts of the circulation. The wall is traditionally divided up into three layers, the innermost (tunica) intima, the (tunica) media, and the outermost (tunica) adventitia. The intima consists of two parts: the endothelium, a single layer of cells, which extends as a

continuous lining to all blood vessels, and, surrounding it, a thin subendothelial layer containing collagen fibres. Outside this is the inner boundary of the media, formed mainly by a layer of inter-linked elastin fibres, called the internal elastic lamina. The rest of the media (usually the thickest part of the wall, and that which dominates its elastic behaviour) has a different structure in large central arteries from that in small arteries. In the former it consists of multiple concentric layers of elastic tissue (elastin), separated by thin layers of connective tissue (collagen) and occasional smooth muscle cells. In smaller arteries, the media consists almost entirely of spirally wound smooth muscle cells, arranged in layers, with small amounts of collagen and elastin between them. The outside of the media in each case consists of a thin, external elastic lamina. The adventitia is often as thick as the media, but is less important mechanically because it consists largely of loose connective tissue, containing relatively sparse elastin and collagen fibres.

The elastin, collagen and smooth muscle fibres constitute about 50% of the material of the wall; the rest is largely water, inside or outside cells, which has a negligible effect on the mechanical properties of the wall apart from being effectively incompressible. In large arteries (of dogs) elastin and collagen together constitute about 50% of the dry mass. In the intrathoracic aorta the ratio of elastin to collagen is about 1.5, while in other arteries it is about 0.5. It should be mentioned that the walls of all arteries larger than about 1 mm in diameter have their own blood supply, through small vessels called the *vasa vasorum*. These originate either from the parent artery or from a neighbour, pass into the adventitia, and break up into a capillary network reaching the inner part of the media. The ratio of wall thickness to internal diameter for every large artery is roughly the same, about 0.06 to 0.08, but increases in muscular arteries below about 1 mm in diameter to a value of about 0.4 in arterioles (diameter 0.1 mm).

The elastic properties of the artery wall clearly depend both on the properties of its individual components and on how they are linked together. Elastin is an easily extensible elastic material, individual fibres having non-linear stress-strain relations (fig. 1.6(a)) with a Young's modulus of about 300 kN m^{-2} for strains up to about 40%, but greater stiffness for larger strains (Carton *et al.*,

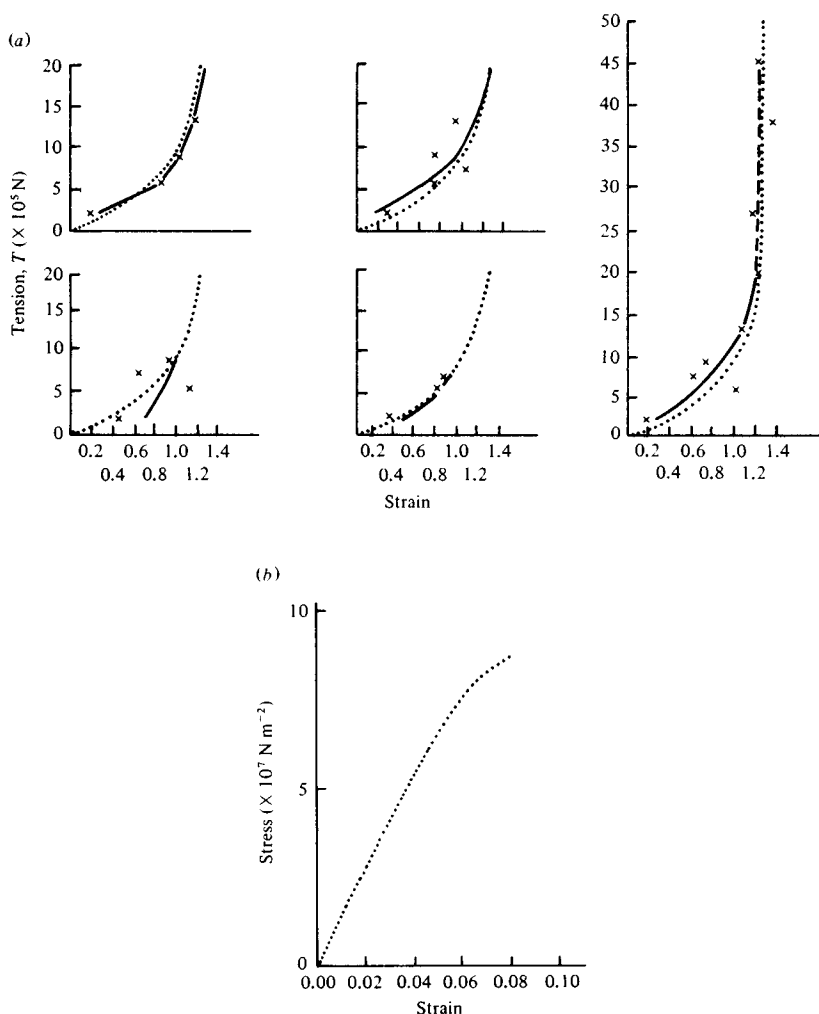


Fig. 1.6. (a) Tension-strain graphs for individual elastin fibres; the dotted curve is a mean curve derived from all specimens. (After Carton *et al.*, 1962.) (b) Stress-strain curve for human tendon, which is made up largely of longitudinally arranged collagen fibres; the curve is the average for over 50 tendons. (After Benedict *et al.*, 1968.)

1962). Collagen is much stiffer, lengths of human tendon having a Young's modulus of about 10^6 kN m $^{-2}$ (fig. 1.6(b)). Smooth muscle has a Young's modulus roughly similar to that of elastin, but its

actual value depends on the level of physiological activity, varying from about 100 kN m^{-2} in the relaxed state to 1200 kN m^{-2} in the active state. Of these three materials, only elastin is purely elastic; both collagen and, especially, smooth muscle show marked visco-elastic properties (creep, stress relaxation and hysteresis), which are reflected in the dynamic properties of artery walls.

As the above description of arterial wall structure shows, the arrangement of the different fibres in the wall is inhomogeneous and very complicated, and to infer the elastic properties of the wall as a whole (regarded, for example, as a thin-walled cylinder) from those of its constituents is virtually impossible. Instead, experiments have been performed on segments of artery, excised from newly dead animals, and with their ends occluded in some way. In these experiments the dimensions which can be accurately measured are length, l , and internal volume, V (or, equivalently if the cross-section is circular, external radius, a_o , linked to internal radius, a_i , by knowledge of the wall thickness, h , which is deduced from a single measured value at particular values of l and a_o , using the assumption of incompressibility; this assumption is accurate for all biological tissue (Patel & Vaishnav, 1972)). In this book the internal cross-sectional area, A , will in general be used as the important transverse dimension; this can be deduced from V and l . The forces tending to deform the artery wall in these experiments are longitudinal tension, T , and transmural pressure, $p_{tm} = p(\text{inside}) - p(\text{outside})$.

Among the first observations to be made are (a) that the length of the artery shrinks by up to 40% of its in-vivo length, l_1 , when it is excised, and (b) that the curve relating p_{tm} to A depends strongly on l (Bergel, 1972*b*). This shows that the artery is normally under considerable tension, and that pressure–area curves measured at lengths other than l_1 have no physiological relevance. All pressure–area relations quoted will be for values of l equal or close to l_1 . Another simple observation is that if l is not held constant, but a constant (usually zero) longitudinal tension is applied, then l increases as p_{tm} increases. This immediately reveals that the elastic properties of the artery wall are not isotropic, since a cylinder made of isotropic material with non-zero Poisson's ratio, σ , would shorten in such circumstances (since artery walls are effectively

incompressible, σ is approximately 0.5). It is more reasonable to take artery walls to be *orthotropic*, with different elastic constants for stresses applied longitudinally than for stresses applied circumferentially (by means of a distending pressure), but with no extra constants to be defined for stresses applied in other directions.

The static elastic properties of an excised artery wall, then, can be defined by plotting p_{tm} against A for fixed l , and T against l for fixed A . Such curves are shown (for the canine thoracic aorta, and the femoral and saphenous arteries respectively) in fig. 1.7. In each case the *dimension* (A or l) is plotted as the ratio of its actual value to its value at average in-vivo conditions (A_0 is the area at a transmural pressure of 13.3 kN m^{-2} , or 100 mmHg, and l_1 is the in-vivo length). In each case the curve is markedly non-linear, with its slope increasing greatly as A or l exceeds its normal mean value. This would not happen in a linearly elastic material, where $p_{tm} \propto 1 - a_{i0}/a_i$ (a_i , a_{i0} being the actual and the initial internal radii), or in rubber, where $p_{tm} \propto 1 - (a_{i0}/a_i)^2$. Such an increase in slope is required for vessel stability; without it 'blow-outs' would commonly occur. In the most frequently quoted experiments, p_{tm} was not taken below about 2.7 kN m^{-2} (20 mmHg) so that the cross-section of the artery remained circular at all times. It has been proposed that the sharp increase in slope of the curves in fig. 1.7 is associated with the fact that, at low strains, the collagen fibres are not taut, and the relatively extensible elastin bears the load; at higher strains, however, the much stiffer collagen fibres increasingly straighten and support the stress. The analogy of a balloon in a string bag is commonly made (Roach & Burton, 1957). This explanation may well be true in part, but the non-linear properties of elastin itself (fig. 1.6(a)) are probably also important.

In order to predict the speed of propagation of the pressure pulse (chapter 2), the important parameter describing vessel wall properties is the distensibility, D , defined by

$$D = (1/A)(dA/dp_{tm}), \quad (1.5)$$

which can be computed directly from data such as that of fig. 1.7(a), measured at in-vivo length (Lighthill, 1975, chapter 12). Despite this, it has been conventional to convert such measurements into an effective incremental Young's modulus, E , for circumferential

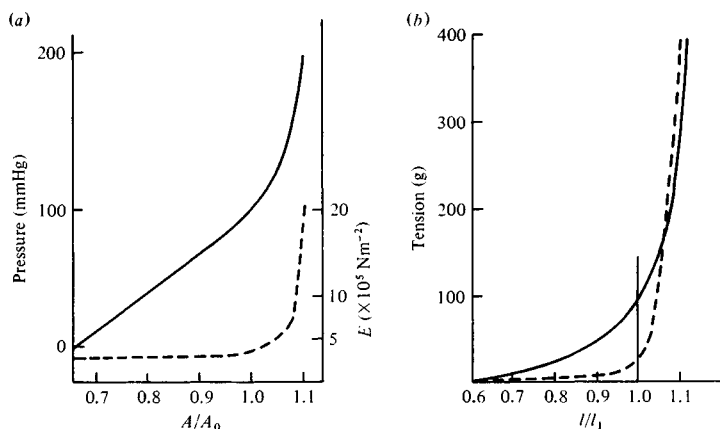


Fig. 1.7. (a) The pressure (continuous curve) and incremental elastic modulus (broken curve) of a segment of dog thoracic aorta, plotted against area divided by in-vivo area ($100 \text{ mmHg} \approx 13.3 \text{ kN m}^{-2}$). (b) Tension-strain curves for longitudinal extension of specimens of femoral (continuous curve) and saphenous (broken curve) arteries of the dog; l_1 is the length *in vivo*. (After McDonald, 1974.)

extensions of the whole vessel wall, modelled as a uniform cylinder with homogeneous, isotropic (or, exceptionally, orthotropic) walls. The use of an incremental Young's modulus is made necessary by the non-linearity of the relation between hoop stress and circumference, so that the only way to define a single elastic parameter is to consider small departures from a mean, prestressed, in-vivo state, and linearise the stress-strain curves. This may be useful if the amplitude of the pressure pulse is not too large. For an increase in pressure within a thin-walled isotropic arterial segment whose length is held constant, E is related to D by

$$D^{-1} = [E/(1 - \sigma^2)] (h/d), \quad (1.6a)$$

where h is the wall thickness, d is vessel diameter and σ is Poisson's ratio, equal to 0.5 since the material is incompressible. This result follows from the classical elasticity of thin shells, and is quoted in a slightly more general form for thick-walled tubes by Bergel (1972*b*). The corresponding result for an orthotropic tube, with different Young's moduli, E_θ , E_x , and Poisson's ratios, $\sigma_{x\theta}$, $\sigma_{\theta x}$, for

applied circumferential or longitudinal stresses, respectively, is

$$D^{-1} = [E_{\theta}/(1 - \sigma_{x\theta} \sigma_{\theta x})](h/d) \quad (1.6b)$$

(Atabek, 1968; Lighthill, 1975). Using formulae such as these, values of E_{θ} have been calculated for many canine arteries, and are given in table 1.1, where it can be seen that arteries become stiffer with increasing distance from the heart; the thoracic aorta has a distensibility of about $0.021 \text{ m}^2 \text{ kN}^{-1}$, while D for the femoral artery is about half this. Values of E_x , the incremental Young's modulus for static longitudinal loading, have also been measured in some vessels; for example, Patel & Vaishnav (1972) quote a value of 670 kN m^{-2} for E_x in the thoracic aorta, while their results give a slightly higher value (740 kN m^{-2}) for E_{θ} , at the upper limit of the range quoted in table 1.1.

The experiments discussed above concern static loading, while the actual transverse loading of an artery as the pressure pulse passes is dynamic, and the viscoelastic wall properties come into play. These have been examined by measuring the changes in cross-sectional area when a sinusoidal pressure oscillation of angular frequency ω is superimposed on the mean level (of 13.3 kN m^{-2}). A linear approximation to the results is given by quoting a *complex* incremental Young's modulus (or distensibility) whose imaginary part represents the viscous element of wall behaviour, causing the oscillations in area to lag behind those in transmural pressure. Thus E or E_{θ} is replaced by $E_{\text{dyn}} + i\eta\omega$ (to use the notation of Bergel (1961*b*) and McDonald (1974)). Experiments show that, for frequencies of 2 Hz or above, both E_{dyn} and $\eta\omega$ are effectively constant, the former at a value that is greater than the static value of E_{θ} by a factor of between 1.1 and 1.7, depending on the artery studied (fig. 1.8), and the latter at a value equal to $0.1\text{--}0.2E_{\text{dyn}}$. For lower frequencies, however, both quantities are frequency-dependent, tending to their static values (E_{θ} and 0 respectively) as $\omega \rightarrow 0$. In the dog the heart-rate is about 2 Hz, so the higher-frequency constant values can be used. In man the heart-rate is about 1.2 Hz; it is not known, however, what the lower end of the frequency-independent range is in man. Patel & Vaishnav (1972) report that the longitudinal dynamic modulus is greater than the transverse modulus by nearly 10% (although the static modulus

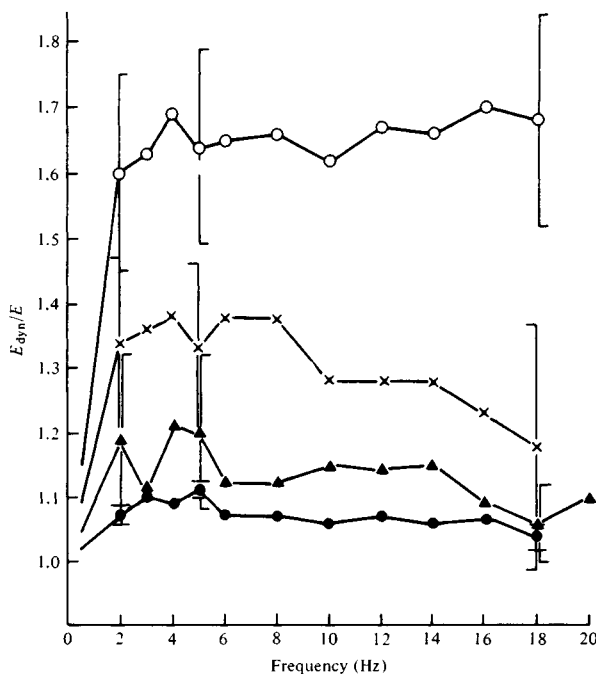


Fig. 1.8. Average values of the dynamic elastic modulus, E_{dyn} , for several arteries expressed as a ratio to the static value, E , plotted against frequency: filled circles, thoracic aorta; filled triangles, abdominal aorta; crosses, femoral artery; open circles, carotid artery. (After Bergel, 1961*b*.)

is smaller by the same amount). The imaginary part, for isolated arterial segments kept *in situ*, is greater by a factor of 3–4 for longitudinal wall motion than for transverse.

There are two main uncertainties involved in using the mechanical properties of isolated arteries for predictions of *in vivo* mechanics. One is the fact that arteries pass through, and are firmly tethered to, the surrounding tissue, the outer boundary of the adventitia being rather ill defined. This tethering has the effect of greatly inhibiting longitudinal wall movements, which actually means that static experiments on segments of artery whose length is held fixed are more likely to be relevant *in vivo* than if considerable longitudinal wall motions were possible. There must also be some constraint on the radial motion, in that the effective inertia, stiffness and viscosity of the wall will all be increased somewhat, especially

the inertia (Patel & Fry, 1966). It is only because wall inertia does not play an important part in pulse-wave propagation (Atabek, 1968) that this radial tethering can be ignored without gross inaccuracy.

The other uncertainty is much more important, and concerns the effect of smooth muscle, which in excised arterial segments is relaxed, but *in vivo* will have an unknown degree of activity; Gow (1972) has devoted a whole chapter to the subject. Three separate effects of smooth muscle contraction can be distinguished. (a) If the artery's diameter is held fixed, contraction of the smooth muscle tends to decrease its distensibility. (b) However, if the distending pressure is held fixed, muscle contraction reduces the diameter, putting the artery onto a less steep part of the pressure–area curve, and the distensibility is increased. (c) The situation *in vivo* is further complicated by the fact that, if all vascular smooth muscle is contracted, including that in the arterioles, the mean arterial blood pressure rises (in order to overcome the increased peripheral resistance), so the net effect on distensibility is unclear. Fortunately, there is a sufficiently small proportion of smooth muscle in the walls of the largest arteries that the effects of its contraction, whether known or not, are small. Otherwise the predictions of pulse-wave velocity made in chapter 2, for example, could not be made. The main influence of smooth muscle is on the viscous behaviour of the wall (Bergel, 1972*b*), and is not known to depend significantly on the state of contraction.

1.1.3 *The pulmonary arteries*

The pulmonary circulation differs from the systemic circulation in several important respects. For example, the mean transmural pressure of large pulmonary arteries is only about 2 kN m^{-2} (as opposed to 13 kN m^{-2} in systemic arteries); the walls of pulmonary arteries are much thinner than those of systemic arteries; and the branching pattern is quite different, many more bifurcations being approximately symmetric, and most of them occurring after only a few (1.5 to 5) diameters of the parent tube (Cumming *et al.*, 1969). The diameter and length of the main pulmonary artery (corresponding to the aorta) in the dog are about 1.7 cm and 3.5 cm respectively; in man the corresponding values are 2.5 cm and

5.0 cm. The main pulmonary artery divides into two arteries supplying the left and right lung, which split into several branches supplying the lobes. These arteries enter the lung itself, and all subsequent arteries are surrounded by a thin sheath of connective tissue and separated from it by fluid. The state of distension of the lung has an important effect on the transmural pressure experienced by pulmonary arteries, and therefore knowledge of it is an essential prerequisite to predictions of the dynamics of the pulmonary circulation. The area ratio of pulmonary branches is less than 1 for two generations, but increases thereafter.

Pulmonary arteries have much thinner walls than systemic arteries of comparable size, h/d taking a value closer to 0.01 than to 0.1. The walls are again usually divided into intima, media and adventitia; the media of all pulmonary arteries of diameter greater than 1 mm consists largely of elastin, with little collagen or smooth muscle. Smaller pulmonary arteries are more muscular, and h/d increases, but only up to a maximum of about 0.1, not 0.4 as in very small systemic arteries. The elastic properties of excised pulmonary arteries have not been as thoroughly studied as those of systemic arteries, but because of their physiological circumstances they have been studied, at least qualitatively, over a wider range of transmural pressures. Fig. 1.9 shows that the main pulmonary artery has a larger Young's modulus than the aorta at transmural pressures typical of the aorta, although the relatively thin wall means that they are not less distensible (see (1.6a) and also table 1.2). At their own normal transmural pressures, however, pulmonary arteries are definitely more distensible than any systemic artery: graphs of pulmonary artery diameter against transmural pressure presented by Maloney, Rooholamini & Wexler (1970) indicate values of D ranging from $0.35 \text{ m}^2 \text{ kN}^{-1}$ for large vessels to $0.88 \text{ m}^2 \text{ kN}^{-1}$ for the smallest. These are over 10 times greater than systemic values. The cross-section of pulmonary arteries remains circular for transmural pressures down to about 1.5 kN m^{-2} , but as p_{tm} is reduced to 0.5 kN m^{-2} , the cross-section becomes markedly non-circular. This can be important *in vivo* because p_{tm} at the top of the lung normally does fall as low as this, and sometimes even becomes negative (see § 1.2). This type of behaviour is discussed more quantitatively in the following subsection, on veins, in which it has been studied in more detail.

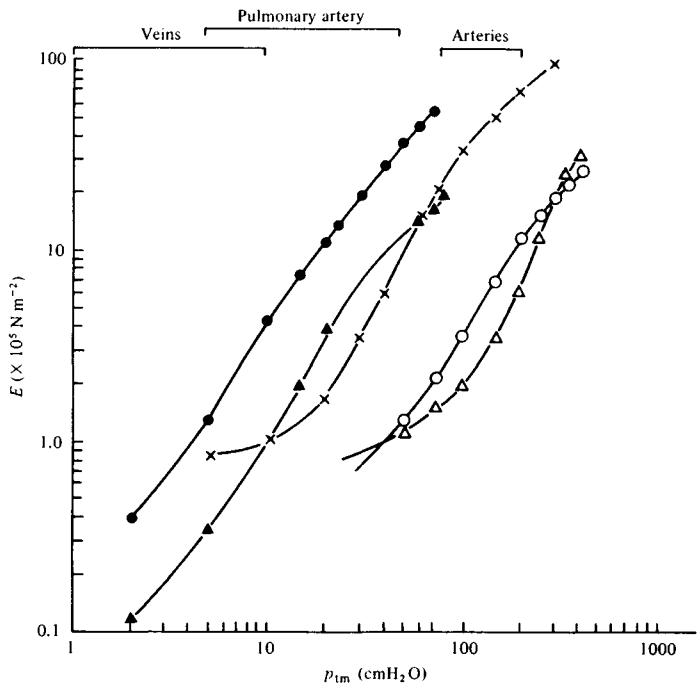


Fig. 1.9. Dependence of effective incremental Young's modulus E on transmural pressure, p_{tm} , for various vessels: filled circles, inferior and superior venae cavae; filled triangles, jugular vein; crosses, pulmonary artery; open circles, descending aorta; open triangles, carotid artery. The normal physiological ranges of transmural pressures for systemic arteries, pulmonary arteries and veins at the level of the heart are also indicated. (After Attinger, 1969.)

Table 1.2. *Distensibility of different vessels at (A) $p_{tm} = 4 \text{ kN m}^{-2}$ and (B) $p_{tm} = 1 \text{ kN m}^{-2}$*

Vessel	$E(\text{kN m}^{-2})$		h/d		$D(\text{m}^2 \text{kN}^{-1})$	
	A	B	A	B	A	B
Venae cavae	3000	420	0.006	0.008	0.04	0.22
Jugular vein	1000	110	0.011	0.015	0.07	0.45
Pulmonary artery	600	106	0.015	0.026	0.08	0.27
Aorta	100	Not given	0.092	0.12	0.08	—

1.1.4 *The veins*

The systemic venous system is not a replica of the arterial system in which the only difference lies in the direction of blood flow. For example, there are many more veins of a given diameter than there are arteries, so that the veins normally contain almost 80% of the systemic blood, although this figure can vary enormously.

Furthermore, the transmural pressures are normally negative in some veins, while they are large and positive in others (see § 1.2), and the walls of veins are much thinner than those of arteries. Many veins in the limbs contain valves, which prevent backflow and probably have an effect on the propagation of pulsatile pressures along the venous system. These valves each have two cusps, with sinuses behind them on the downstream side. No survey has been made, as far as I know, of area ratios and branching angles in the veins.

Three layers can be described in the walls of medium and large veins, as in arteries; they are all much thinner, however. The intima consists of the endothelium and only a small amount of elastin. The media consists essentially of a few layers of spirally wound smooth muscle, interspersed with a little elastin and collagen; it is the absence of large quantities of elastin in the media that constitutes the primary structural difference between veins and arteries. The smallest veins do not contain significant smooth muscle. Veins in parts of the body normally below the heart have relatively thick media, though whether this is because they experience a relatively high transmural pressure is not known. In veins the major wall compartment is the adventitia, which contains a network of elastin and collagen fibres, but principally the latter (the ratio of elastin to collagen is about 0.3 in the largest veins, compared with 0.5–1.5 in arteries). The thickness-to-diameter ratio of veins is about 0.01, like that of pulmonary arteries.

The elastic properties of veins have not been studied systematically. The most thorough investigation of a single type of vein is that by Moreno *et al.* (1970) on the inferior vena cava of a dog. Fairly detailed measurements on both venae cavae and the jugular vein (also of a dog) are reported by Attinger (1969). Moreno *et al.* realised that many veins commonly experience both positive and negative transmural pressures, and therefore studied the pressure–

area relations of excised segments of vein over a wide range of such pressures. They also compared their results with those obtained from rubber tubes of comparable diameter and wall thickness; this is important because many model experiments on flow in collapsible tubes, intended as an indication of how veins might behave, are performed with rubber tubes (see chapter 6).

Fig. 1.10(a) shows the results of this experiment, while fig. 1.10(b) shows the relation between area and perimeter. From these graphs and from observations of the shape of the cross-section of the tube, we can describe the elastic behaviour of the tubes as p_{tm} is reduced from 4 kN m^{-2} (30 mmHg). When p_{tm} exceeds about 1.5 kN m^{-2} the cross-section of the vein is circular, and the wall is very stiff. In fact $D \approx 0.04 \text{ m}^2 \text{ kN}^{-2}$ when $p_{tm} = 4 \text{ kN m}^{-2}$ which is less than that of arteries at the same p_{tm} , although the wall is much thinner, because the collagen (in the adventitia) becomes fully extended at a lower p_{tm} than in arteries. This is best deduced from the results of Attinger (1969), who plots values of E (see fig. 1.9) and h/d for veins, pulmonary arteries and systemic arteries at various pressures. His values for $p_{tm} = 4 \text{ kN m}^{-2}$ and 1 kN m^{-2} , and the corresponding values of D calculated using (1.6a), are given in table 1.2. Changes in cross-sectional area are accompanied by appropriate changes in perimeter (proportional to $A^{1/2}$). As p_{tm} is reduced from 1.5 to 1.0 kN m^{-2} , the vessel still remains circular, but becomes somewhat more distensible, presumably because the elastin or smooth muscle in the wall takes over from the collagen. When p_{tm} falls below about 1.0 kN m^{-2} , the vessel becomes elliptical, the area falls more rapidly, and the distensibility rises. The perimeter also continues to fall, although no longer as $A^{1/2}$, and it is this reduction in perimeter, not the change in cross-sectional shape, that makes the larger contribution to the reduction in area (and hence to the distensibility) at least while p_{tm} exceeds about 0.5 kN m^{-2} . As p_{tm} falls below this value, however, the change in shape becomes more marked, and makes an increasing contribution to D , which has a maximum of about $3.5 \text{ m}^2 \text{ kN}^{-1}$ when p_{tm} is slightly below 0.5 kN m^{-2} . From then on, the slope of the graph falls again. When p_{tm} falls below about -0.1 kN m^{-2} , the vessel cross-section becomes increasingly distorted from its elliptical shape, until at a p_{tm} of -1.0 kN m^{-2} it is almost completely collapsed, in the dumb-

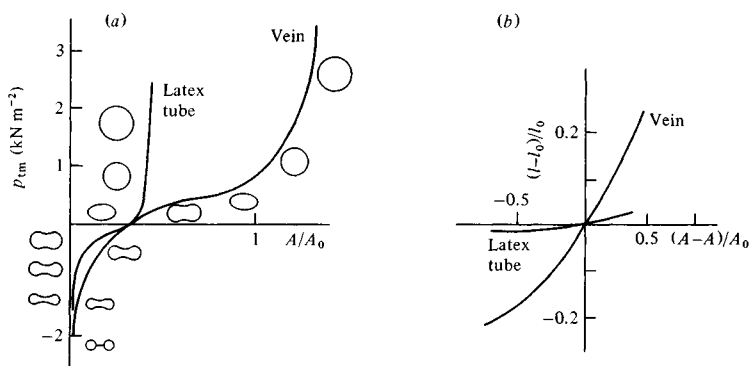


Fig. 1.10. Comparison of the elastic properties of a latex tube with those of an excised segment of a canine vena cava. (a) Transmural pressure as a function of area, A , scaled with respect to the area at zero transmural pressure, A_0 . Transverse cross-sections are shown for various areas. (b) Perimeter as a function of cross-sectional area. (Data from Moreno *et al.*, 1970.)

bell configuration shown. The two side-channels may be more nearly closed than shown, because in this state the endothelium becomes corrugated and the cells tend to protrude into the vessel. In this configuration D is again very low, tending to 0 as $A \rightarrow 0$, because A is constrained to be greater than, or equal to 0.

The graphs presented by Moreno *et al.* (1970) indicate that there is a second peak in D at a negative value of p_{tm} , because A (see (1.5)) has become small more rapidly than dA/dp_{tm} . However, this may not be a real phenomenon, because of the difficulty of measuring very small areas and pressures accurately. Note that a number of workers use the term *distensibility* to describe the quantity

$$D' = (1/A_0)(dA/dp_{tm}), \quad (1.7)$$

where A_0 is a reference area, for example the value of A when p_{tm} is 13.3 kN m^{-2} ($= 100 \text{ mmHg}$). This 'pseudo-distensibility' is close to the true distensibility if all areas considered are close to A_0 , as for systemic arteries under physiological conditions, but is quite different when a wide range of areas is considered, as here.

It is interesting to note the corresponding behaviour of the rubber tube. The cross-section remains circular until p_{tm} falls almost to 0, and then becomes elliptical and, later, dumb-bell shaped like a vein. However, during collapse, the perimeter of the rubber tube remains almost constant (fig. 1.10(b)), and the area change is associated solely with change of shape. Furthermore, the maximum rate of change of area occurs at a negative value of p_{tm} (about -0.25 kN m^{-2}), while that of a vein occurs at a positive value. It can also be seen that the slope of the graph in fig. 1.10(a) changes much less abruptly for a vein than for a rubber tube, because of the continuing change in perimeter.

The reason for this difference in elastic properties (fully analysed by Moreno *et al.* (1970)) lies in the fact that the effective Young's modulus of the rubber tube for deformations to an unstressed state, about 2100 kN m^{-2} , is about 40 times that of the vein. Therefore the wall resists both stretching (hence the constant perimeter once collapse has begun) and bending more firmly than in veins. It is the resistance to bending at the points of maximum curvature that provides the stiffness of the collapsed state: the bending moment required to maintain radius of curvature R in a slender beam of breadth b and thickness h (i.e. part of a segment of the vessel wall, sliced longitudinally and of axial length b) is proportional to Ebh^3/R , increasing with E for constant values of b , h and R . This provides a qualitative explanation for the results. A more quantitative explanation was also provided by Moreno *et al.* (1970), using the analysis described by Love (1927, pp. 423–4) for a bent, linearly elastic rod (or longitudinally uniform cylinder), which leads to the following differential equation for the shape of the cross-section $y(x)$, using the coordinate system of fig. 1.11:

$$-y''/(1+y'^2)^{3/2} = [\frac{1}{2}p_{tm}(x^2+y^2) + k]/EI, \quad (1.8)$$

where $I = h^3/12$ is the moment of inertia of the cross-section per unit length of tube, and k is a constant. Equation (1.8) is solved numerically, subject to the boundary conditions that $y(x)$ and $y'(x)$ should be periodic, and k is determined by knowing either the perimeter or the cross-sectional area at a particular value of p_{tm} . Moreno *et al.* showed how their numerical solutions gave good agreement between theory and experiment for the relations

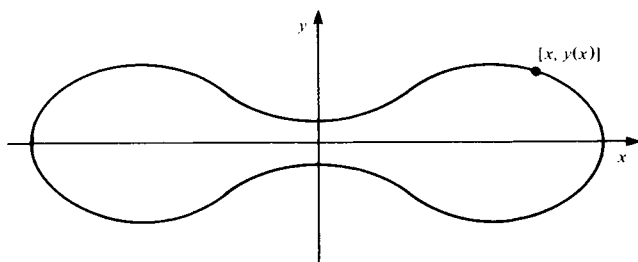


Fig. 1.11. Coordinate system for the buckled cross-section of an elastic tube.

between p_{tm} , A , perimeter and shape, for both rubber tubes and veins.

Other analyses (e.g. Flaherty, Keller & Rubinow, 1972*a*) have analysed the buckling of elastic cylinders in more detail, and have demonstrated that if the wall is very thin, it does not begin to buckle elliptically, but in a periodic shape with circumferential wave number greater than 2, this number increasing as h/d decreases. This accords with experiment (J. M. Fitz-Gerald, personal communication).

The fluid mechanical consequences of the great distensibilities and shape changes of venous cross-sections have not been fully worked out. Model experiments designed to elucidate them, and some preliminary theoretical analysis of these experiments, are described in chapter 6.

Finally, mention should be made of pulmonary veins, which, like pulmonary arteries, were examined by Maloney *et al.* (1970). They have a structure similar to that of systemic veins, and distensibilities of between 0.17 and $0.35 \text{ m}^2 \text{ kN}^{-1}$, which are slightly less than those of similarly sized pulmonary arteries at similar transmural pressures ($1\text{--}2 \text{ kN m}^{-2}$), and comparable with those of systemic veins (see table 1.2).

1.1.5 The blood

We conclude this section with a very brief description of the mechanical properties of blood. Much more detail can be found in Whitmore (1968), Charm & Kurland (1972), Cokelet (1972) and Caro *et al.* (1978, chapter 10). Blood is a suspension of formed

elements in plasma. The formed elements, which normally occupy about 45% by volume of the blood (a proportion which is slightly species- and sex-dependent), are the red cells, white cells and platelets. Red cells are by far the most numerous, and completely dominate the mechanical properties. They are flexible, biconcave discs, of diameter about $8\text{ }\mu\text{m}$ (in most mammals) and thickness about $1\text{ }\mu\text{m}$ at the centre and $2\text{--}3\text{ }\mu\text{m}$ at the edge; there are about 5 million red cells per cubic millimetre of whole blood. The white cells are on the whole slightly larger, and equally deformable, but are far less numerous (1–2 white cells per 1000 red cells) and therefore dynamically unimportant. The platelets are more numerous than white cells (80–100 per 1000 red cells), but are very small, rounded cells of diameter $2\text{--}4\text{ }\mu\text{m}$. They too are normally unimportant dynamically, but they react very strongly with foreign substances, and therefore play a significant role in the process of blood clotting, as well as being involved in the later stages of the development of atherosclerosis. The plasma is a solution of large molecules, but on the scales of motion and at the rates of shear normally encountered in the blood vessels, it can be regarded as a homogeneous Newtonian fluid of viscosity $0.0012\text{--}0.0016\text{ kg m}^{-1}\text{ s}^{-1}$ at body temperature (37°C).

Whole blood cannot be regarded as a homogeneous fluid in the smallest blood vessels, because the diameters and spacing of red cells are comparable with capillary diameters. However, in vessels whose diameters exceed $100\text{ }\mu\text{m}$, blood can be regarded as effectively homogeneous, because the scale of the microstructure is so much smaller than that of the flow. The remaining question to be answered is whether blood can also be assumed to be Newtonian in the large vessels. The standard test of this is to place a quantity of blood in a constant-shear viscometer and to measure its effective viscosity as a function of shear-rate, S . It is found that the measured viscosity is independent of S for $S > 100\text{ s}^{-1}$ (Whitmore, 1968). We shall see in chapter 3 that the average shear-rate at the walls of arteries is significantly greater than this, and on that basis we shall assume blood to be Newtonian, although it is clear that near the centre of a straight vessel, or in separated regions of recirculating flow, the average value of S will be small. Furthermore, even the wall shear passes through zero twice per cycle (as it reverses), so it is

not true that $S > 100 \text{ s}^{-1}$ everywhere at all times. It is not clear how to assess the importance of temporarily non-Newtonian blood on unsteady arterial fluid dynamics; this is a problem that should be investigated, but that will here be ignored. We take blood to be a homogeneous Newtonian fluid of density $1.05 \times 10^3 \text{ kg m}^{-3}$, viscosity $0.004 \text{ kg m}^{-1} \text{ s}^{-1}$ (at 37°C) and hence kinematic viscosity about $4 \times 10^{-6} \text{ m}^2 \text{ s}^{-1}$.

1.2 The physiological relevance of fluid mechanics

In this section, I first outline those physiological phenomena that a fluid mechanical analysis might hope to explain, and then quote the experimental results which suggest that the shear stress exerted by the flowing blood on the artery wall is an important factor in the development of arterial disease.

1.2.1 *Blood pressure and transmural pressure*

The pressure in the blood at any location is made up of three components: (i) atmospheric pressure, p_0 , which is normally taken to be the pressure in the right atrium when its muscles are relaxed; (ii) the hydrostatic pressure, $-\rho gh$, where h is the vertical distance above the right atrium and ρ is the density of the blood; and (iii) the pressure generated by the heart, which we shall denote by p (Lighthill (1975) calls this component the 'excess pressure'). This last component is alone responsible for the motion of the blood, and is commonly called 'blood pressure' (blood pressure is always measured clinically 'at the level of the heart'); p has a mean value of 13.3 kN m^{-2} in the large arteries, but falls dramatically in the microcirculation, so that the mean pressure in the venae cavae is less than 0.6 kN m^{-2} , and in the right atrium it is even closer to zero.

The pressure p_0 relative to which blood pressures are measured should not be exactly atmospheric, but should be taken to be the pressure inside the chest, which varies with respiration and is normally subatmospheric (by as much as 2 kN m^{-2}) when the lung is expanded. This is because contraction of the ventricular muscle generates a *transmural pressure* between the inside and the outside of the ventricle, the outside being within the chest.

The hydrostatic component of pressure, $-\rho gh$, is important because it determines the transmural pressure of the blood vessels and hence, through their elastic properties (§ 1.1), their calibre. The pressure outside most blood vessels (with the exception of those in the chest and in the skull; see below) is close to atmospheric (in fact, about -0.25 kN m^{-2} ; see Wiederhielm, 1972), so p_{tm} is in most cases approximately equal to $p - \rho gh$. Consider a standing man: the mean transmural pressure is about 13 kN m^{-2} at the entrance to the aorta, and about 0.5 kN m^{-2} at the exit from the venae cavae. In the large vessels of the foot (1.1 m below) these values will be increased by about 11 kN m^{-2} , so that both types of vessel will be distended, will have circular cross-section, and will be very stiff (the transmural pressures in some veins can be reduced by voluntary contraction of the skeletal muscles outside them, and can be further alleviated by the action of the valves). In vessels 30 cm above the heart, however (for example in a raised arm), p_{tm} is reduced by 3 kN m^{-2} . This has little effect on arteries, which remain fully open; veins, on the other hand, experience a negative transmural pressure, and collapse therefore occurs (§ 1.1). Venous return is maintained, either continuously, through the small side-channels, which may not completely close (fig. 1.10), or intermittently, as the build-up of upstream pressure forces the veins open. (I am aware of no measurements that unequivocally demonstrate how this venous return is accomplished.) Veins in the skull do not collapse, because the skull acts as a rigid box, any fall in venous volume being accompanied by a corresponding fall in extravascular pressure.

The transmural pressures experienced by pulmonary blood vessels are more difficult to evaluate, because they depend in a complicated way on the state of lung inflation. We consider only arteries and veins; pulmonary capillaries experience different transmural pressures, but are outside the scope of this monograph. The vessels are surrounded by, and probably also linked (by fibres) to, a continuous perivascular sheath; the space between sheath and vessel wall is filled with fluid. The pressure in this fluid, p_{pv} , differs from air pressure in the alveoli of the lung, p_{alv} , for a number of reasons. First, if the neighbouring alveoli are inflated, the alveolar membranes pull outwards on the perivascular sheath, which effectively reduces p_{pv} by an 'elastic stretching pressure', p_{es} .

However, this effect is itself reduced by the elastic recoil pressure of the perivascular sheath itself, less the effective outwards pressure exerted on the vessel wall by the elastic linkages (if any) that span the perivascular space, a net reduction which we may call p_{er} . Thus

$$p_{pv} = p_{alv} - p_{es} + p_{er}.$$

In a static, uniform lung, in which all alveoli are equally inflated, both p_{alv} and p_{es} will be uniform, and p_{pv} will differ from the pressure in the pleural space which surrounds the whole lung, p_{pl} , only insofar as the elastic recoil pressure of the pervascular sheath, p_{er} , differs from that of the pleural membranes. It is common to assume that p_{pv} is equal to p_{pl} , which can be approximately measured by recording the pressure in a balloon inflated in the aoesphagus. In a normal man, the average value of p_{pl} is about -0.5 kN m^{-2} , i.e. 0.5 kN m^{-2} below atmospheric, when his respiratory muscles are relaxed. This quantity can be decreased to about -3 kN m^{-2} in a very deep inspiration, or increased to more than 6 kN m^{-2} during a forced expiration. In the living animal the lungs are normally not uniformly inflated, because of the effect of gravity: p_{pl} (and hence p_{pv}) decreases with height by approximately 25 N m^{-2} per cm (in man). In any discussion of the state of distension of pulmonary blood vessels it is important to record (or at least estimate) the perivascular pressure as well as the internal pressure.

1.2.2 *Unsteady pressures*

The (excess) pressures measured simultaneously in the left ventricle and in the ascending aorta immediately downstream of the aortic valve are shown in fig. 1.12, where the corresponding graphs for the right ventricle and main pulmonary artery are also shown. The left ventricular pressure rises rapidly at the beginning of systole, and soon exceeds that in the aorta so that the valve opens and ejection begins. About half-way through ejection, the two traces cross, so that an adverse pressure gradient is established across the valve, which decelerates the outflow and is maintained as the two pressures fall. The kink in the aortic pressure curve (the 'dicrotic notch') marks the closure of the valve, and thereafter the ventricular pressure falls rapidly as the heart muscle relaxes, while aortic pressure falls more gradually as blood flows out peripherally.

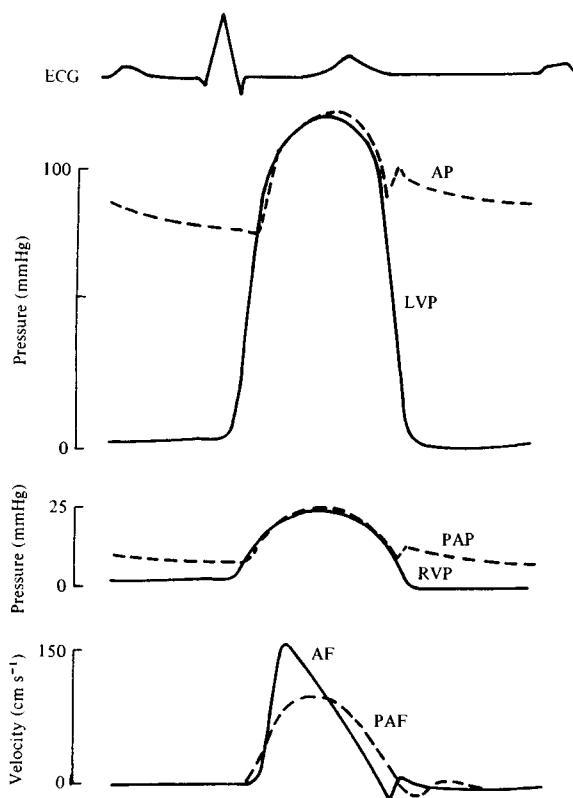


Fig. 1.12. Semi-diagrammatic illustration of pressure and flow-rate occurring simultaneously on the left and right sides of the heart during the cardiac cycle. ECG, electrocardiogram; AP, aortic pressure; AF, aortic flow; LVP, left ventricular pressure; PAP, pulmonary artery pressure; PAF, pulmonary artery flow; RVP, right ventricular pressure. (After Caro *et al.*, 1978.)

Fig. 1.13 shows measurements of pressure made instantaneously at a number of sites along the aorta. The pulse is seen to be increasingly delayed with increasing distance down the vessel, indicating that it is propagated along the aorta as a *wave*. We also note that the shape of the pressure pulse changes dramatically as it propagates: the amplitude increases, the front becomes steeper, and the dicrotic notch disappears. The mean pressure falls, but only very gradually (by about 0.5 kN m^{-2} along the whole aorta). These changes continue as the pulse wave passes into other large arteries

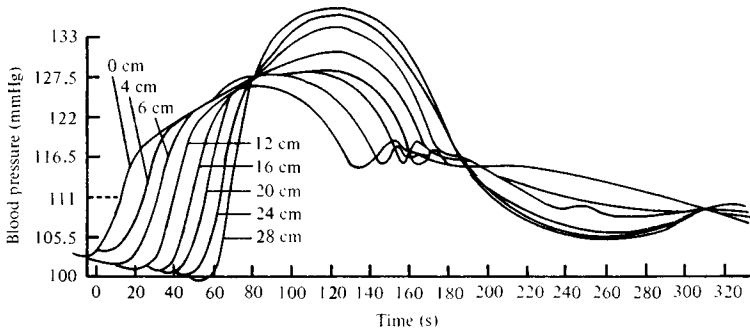


Fig. 1.13. Instantaneous blood pressure records made at a series of sites along the aorta in the dog. 0 cm is at the start of the descending aorta. (After Olson, 1968.)

(fig. 1.14(a)), and it is only in small arteries, with a diameter below about 1 mm, that the amplitude (and the mean) of the pressure pulse begins to fall rapidly. The propagation of the pulse wave is analysed mathematically in chapter 2; the object of any such analysis must be to explain the observed changes.

The pressure waveforms in systemic veins are shown in fig. 1.15; these traces were measured successively at different sites along the same pathway of the same animal. The oscillations in the vena cava are similar to those commonly recorded in the right atrium, and the phase differences between the successive traces clearly reflect the propagation of a wave along the veins from the heart, against the direction of blood flow. The oscillations are almost completely absent in the brachial vein (fig. 1.15(d)), which is almost certainly because there is a valve between that measuring site and those closer to the heart. The role of valves in eliminating pressure oscillations in veins has not been systematically explored. Incidentally, small-amplitude oscillations are observed in very small veins, and are thought to be the attenuated remnants of the arterial pulse. Their amplitude is greater in conditions of vasodilatation, when the microcirculatory attenuation is less severe (see chapter 2; and Zweifach, 1974).

Typical pressure waveforms recorded in the main pulmonary artery and the left atrium (representative of large pulmonary veins) of a dog are shown in fig. 1.16. The former has a similar shape to the

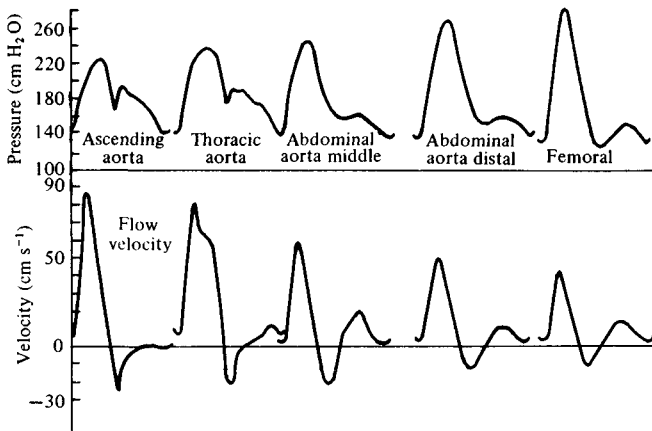


Fig. 1.14. Matched records of (a) pressure and (b) average velocity at different sites in the arteries of a dog. (From McDonald, 1974.)

aortic waveform (albeit with much smaller amplitude), but there is a marked difference between the waveforms in smaller pulmonary arteries (not shown) and those in smaller systemic arteries (fig. 1.13), because there is no obvious change in shape as the wave propagates along the pulmonary arteries.

1.2.3 Velocity waveforms

At any location in the cardiovascular system, the motion of the blood is driven by the local pressure gradient, which in turn is determined by the propagation of the pressure pulse. Thus the fluid mechanical problems of the circulation can be divided into two parts: first, an explanation of the pressure waveforms already described, which is embarked on in chapter 2; secondly, an analysis of the blood motions driven by the pressure gradients, which is introduced in chapter 2, but forms the main subject of chapters 3 to 5. Here, however, we describe measurements of blood velocities.

It was only in the 1960s that it became possible to measure blood velocities or flow-rates in arteries with any degree of confidence. The most common device used on animals was (and still is) the cuff electromagnetic flowmeter. This is placed round a vessel, a uniform transverse magnetic field is applied across the vessel, and the e.m.f. generated in a perpendicular direction when the conducting blood

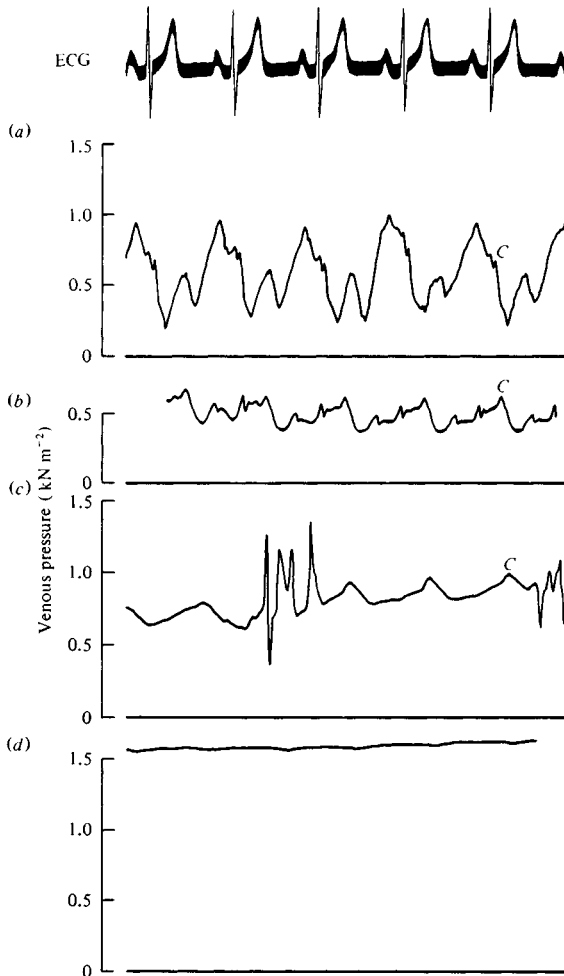


Fig. 1.15. The pressure waveforms measured sequentially with a single catheter at four successive sites in the human venous system. These sites are, from (a) to (d), the superior vena cava, the subclavian vein, the axillary vein and the brachial vein. The four waveforms are aligned with the ECG record (top trace) so that the phase difference between the vena cava and the subclavian vein can be seen; *C* represents the same event in successive records. (After Caro *et al.*, 1978.)

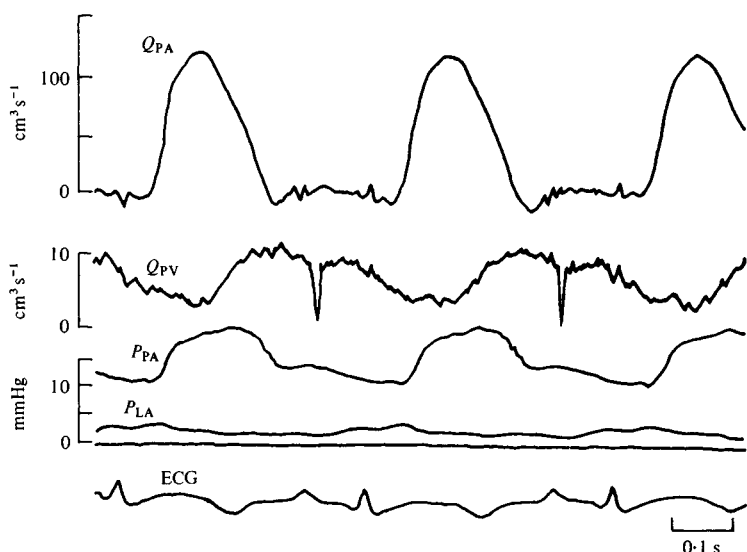


Fig. 1.16. Experimental records of pulmonary pressures and flow-rates in a conscious dog, at rest. Q , blood flow-rate; P , pressure; PA, pulmonary artery; PV, pulmonary vein, within 2 cm of left atrium; LA, left atrium; ECG, electrocardiogram. The sharp spikes in the flow-rate traces during diastole are artefacts. (From Milnor, 1972.)

flows is measured. From it can be inferred the volume flow-rate in the vessel or, equivalently, the average velocity (averaged across the cross-section) as long as the internal diameter of the vessel is known. The cuff flowmeter is reliable as long as the velocity profile in the vessel is axially symmetric (although it does impose some restriction on the radial motion of the vessel wall and therefore might interfere with pulse propagation), and can, in principle, be made insensitive to asymmetries in rectilinear flow (Bevir, 1970). Mills (1972) discusses the operation of these flowmeters in detail. Mills & Shillingford (1967) also designed a catheter-tip electromagnetic flowmeter, which effectively averages the velocity over a small region near the probe and can therefore measure velocities at points within the vessel, as long as the velocity profile is locally approximately flat. A more satisfactory device for the measurement of local velocities is the hot-film anemometer, because it effectively averages over a *very* small region and does not require a flat profile.

This was originally developed and used for blood measurements by three different groups (Ling *et al.*, 1968; Schultz *et al.*, 1969; Seed & Wood, 1970a). The principles of operation of such an anemometer are analysed in the appendix, where particular attention is paid to the behaviour of the probe in unsteady flow. Another method for measuring local velocities is the pulsed ultrasonic Doppler flowmeter (Peronneau *et al.*, 1969); this is, in principle, better than any because it does not require invasion of the blood vessel by a probe, but it has not yet been widely used. The measurements to be presented below are either of average velocity/flow-rate (recorded with a cuff electromagnetic flowmeter) or of local velocity in the centre of the vessel (recorded with a hot-film or a catheter-tip electromagnetic probe). The two will be approximately the same if, and only if, the velocity profile is effectively flat over most of the vessel cross-section, with only thin boundary layers at the wall. In the largest vessels this is indeed the case.

Average velocity waveforms at the entrances of the aorta and the pulmonary artery are given in fig. 1.12, and the variation in the waveform with distance along the systemic arterial tree is depicted in fig. 1.14(b). Blood is ejected from the heart for about one-third of the period of the beat (this fraction increases to about one-half at higher heart-rates), and the ejection phase is followed by a brief period of backflow as the aortic valve closes. The amount of backflow increases with distance from the heart, since it can be accommodated by expansion of that part of the aorta between the measurement site and the heart. The small backflow at the entrance to the aorta can be accounted for by the closed aortic valve bulging back (there is normally negligible leakage) and by diastolic flow into the coronary arteries. The shape of the velocity waveform and its variation with distance must also be explained by an analysis of the pulse wave (chapter 2). Mean and peak velocities in different canine vessels are given in table 1.1; the maximum velocity in the aorta normally exceeds the mean by a factor of 5 or 6. Note that the word 'mean' is used to refer to a time mean, and the word 'average' to denote a cross-sectional average. A sequence of point-velocity waveforms, measured in the centres of the arteries in question with a catheter-tip electromagnetic probe, is shown in fig. 1.17 with the corresponding pressure waveforms. Their general features

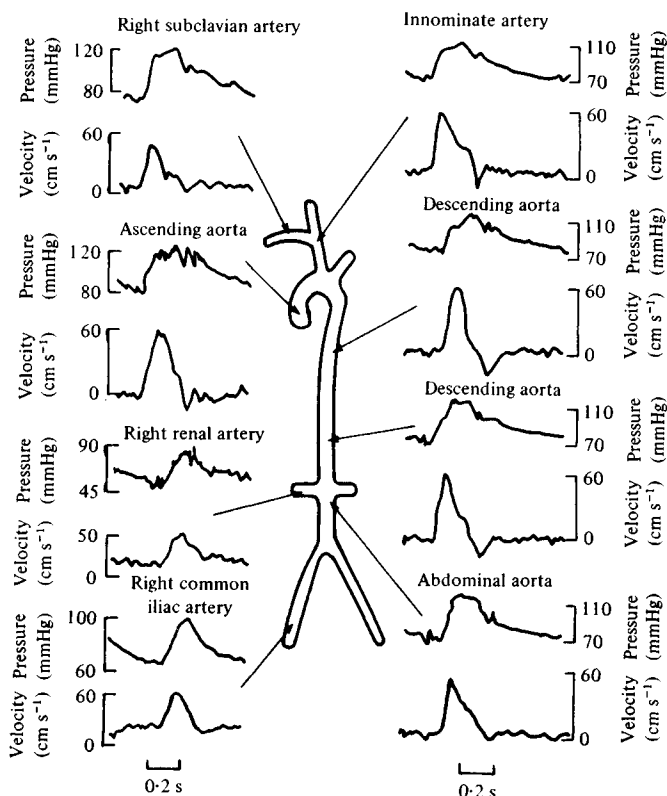


Fig. 1.17. Simultaneous pressure and blood velocity waveforms at numerous points in the human arterial tree. All were taken from one patient with the exception of the right renal artery and the right common iliac artery. (After Mills *et al.*, 1970.)

correspond to those of fig. 1.14(b), but show more fluctuation, suggesting that the high-frequency components of the waveforms are averaged out by the cuff flowmeter.

Velocity waveforms in coronary arteries are different from those in other systemic arteries because of their special circumstances. During systole, when the velocity in the aorta becomes very large, the ventricular muscle is contracted, squeezing the coronary blood vessels within it. Their resistance to flow is therefore very large, and flow is sluggish. In diastole, however, the ventricular muscle is relaxed, the coronary vessels open wide, and a vigorous flow

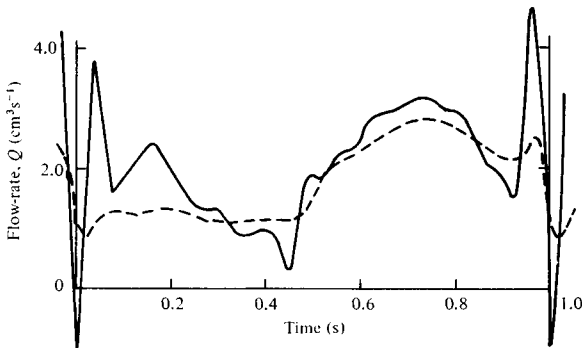


Fig. 1.18. Flow-rate waveform in the left circumflex coronary artery of a dog; continuous curve is predicted from measured pressure gradient, broken curve is measured directly with a cuff electromagnetic flowmeter. (After Atabek *et al.*, 1975.)

through them is established. A measured flow-rate waveform showing this (in a dog) is presented in fig. 1.18. Point-velocity measurements in the same arteries of horses reveal a further interesting phenomenon which is absent in dogs. This is shown in fig. 1.19, indicating relatively high-frequency (10 Hz) and large-amplitude oscillations superimposed on the basic waveform. Their presence in horses has been confirmed by another group of workers (Wells *et al.*, 1974), and the search for a satisfactory explanation is still going on. An intriguing question is whether these oscillations depend on large size, and if so, whether or not they are normally present in man.

Typical flow-rate waveforms in the pulmonary artery and pulmonary vein are shown in fig. 1.16. Data on the average velocity waveforms in the venae cavae (of man) are presented in fig. 1.20, which shows that in each cardiac cycle there are two main oscillations in flow velocity, out of phase with the pressure oscillations: one when the ventricles contract and one when they are relaxed. The contraction of the right *atrium* is associated with low velocities in the venae cavae.

Before turning to velocity profiles, it is worth noting that both pressure and velocity waveforms, being essentially periodic, can be subjected to Fourier analysis. This makes analysis of the relation

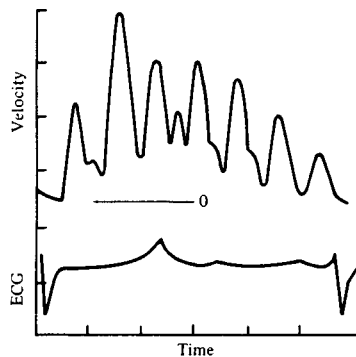


Fig. 1.19. Centre-line velocity waveform in the left circumflex coronary artery of a horse; note the relatively high-frequency oscillations, absent in fig. 1.18. Peak Reynolds number $\bar{Re} = 308$, $\alpha = 3.16$. (After Nerem *et al.*, 1974*b*.)

between the two waveforms particularly simple as long as a linear theory is applicable, and it is shown in chapter 2 that such is normally the case. Patel, de Freitas & Fry (1963*a*) demonstrated that the pressure waveform could be very accurately described with a mean and six periodic components, while 10 periodic components were necessary for comparable accuracy of the flow-rate waveform. This means that velocity probes must be able to respond accurately to frequencies up to 20 Hz (in dogs – only about 12 Hz in man). We may note in passing that a probe designed to measure the wall shear-rate (which involves differentiation of the velocity) must be accurate up to about 100 Hz (50 Fourier components). This is shown in § 3.1, where the difficulties of designing a suitable wall shear probe are briefly discussed.

1.2.4 Velocity profiles

Velocity profiles have been measured in a number of arteries using a hot-film anemometer, with the film mounted on a needle inserted through the artery wall and carefully positioned, but I know of no such measurements in veins. The artery most commonly studied is the canine aorta (Ling *et al.*, 1968; Schultz *et al.*, 1969; Seed & Wood, 1971; Clark & Schultz, 1973), because it is the only one, in a dog, to have an internal diameter greater than about 1 cm; the probes are usually 1–2 mm across, and in any smaller artery they

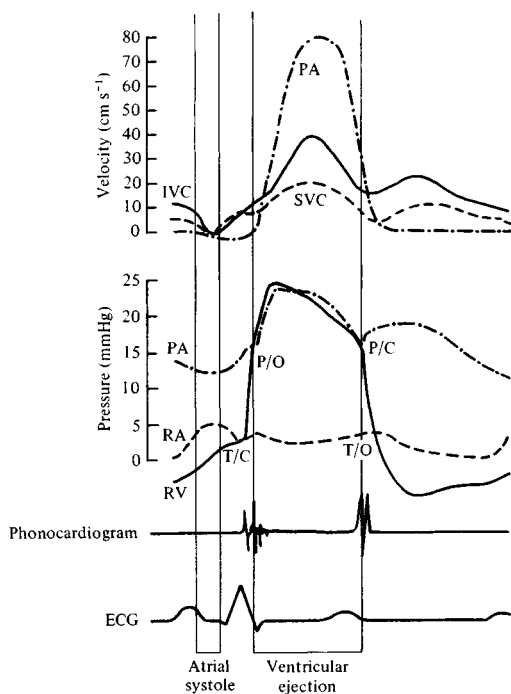


Fig. 1.20. A composite diagram of pressure and velocity of flow into and out of the right side of the heart, constructed from a number of different measurements. The top curves show the velocities in the inferior and superior venae cavae (IVC, SVC) and the pulmonary artery (PA), then come the pressures in the right side of the heart (RA, RV) and pulmonary artery, and then the phonocardiogram and ECG. These are included to serve as timing references. T/C, tricuspid valve closed; P/O, pulmonary valve open; P/C, pulmonary valve closed; T/O, tricuspid valve open. (After Wexler *et al.*, 1968.)

would distort the flow, making accurate measurement of the velocity profile impossible. A few measurements in relatively smaller vessels have been made in the horse (Nerem *et al.*, 1974a). The recording of velocity profiles is complicated, because the profiles vary throughout the cardiac cycle, and care has to be taken in recording velocities at different positions in the vessel cross-section, but at the same stage of the cycle.

The mean velocity profiles at various stations in the canine aorta are presented in fig. 1.21. They can be seen to be roughly flat

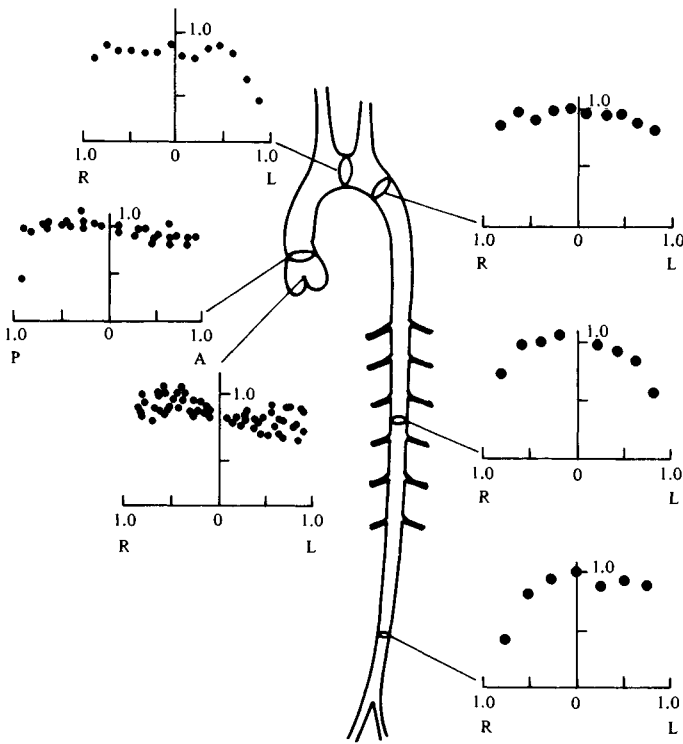


Fig. 1.21. Mean velocity profiles in the aorta of a dog. For each graph, the mean velocity at each site on the vessel diameter is expressed relative to the centre-line mean velocity (ordinate), and positions on the diameter are scaled with respect to the vessel radius (abscissa). R, L: right, left; P, A: posterior, anterior. (After Schultz, 1972.)

throughout, although a relatively thick boundary layer is apparent in the abdominal aorta. Because of the size of the probe and the motion of the artery wall as the wave passes, accurate measurements closer than 1–2 mm from the wall are unobtainable. The same observation, of a fairly flat profile surrounded (one infers) by thin boundary layers, is made throughout the cycle in the ascending aorta (fig. 1.22(a)). Near the aortic valve, the profile remains symmetric, but as the flow enters the arch, a marked skew develops during peak forward flow, with higher velocities towards the posterior wall of the aorta, which is the inside of the curve (fig. 1.22(a) and (b), from measurements made by W. A. Seed and N. B.

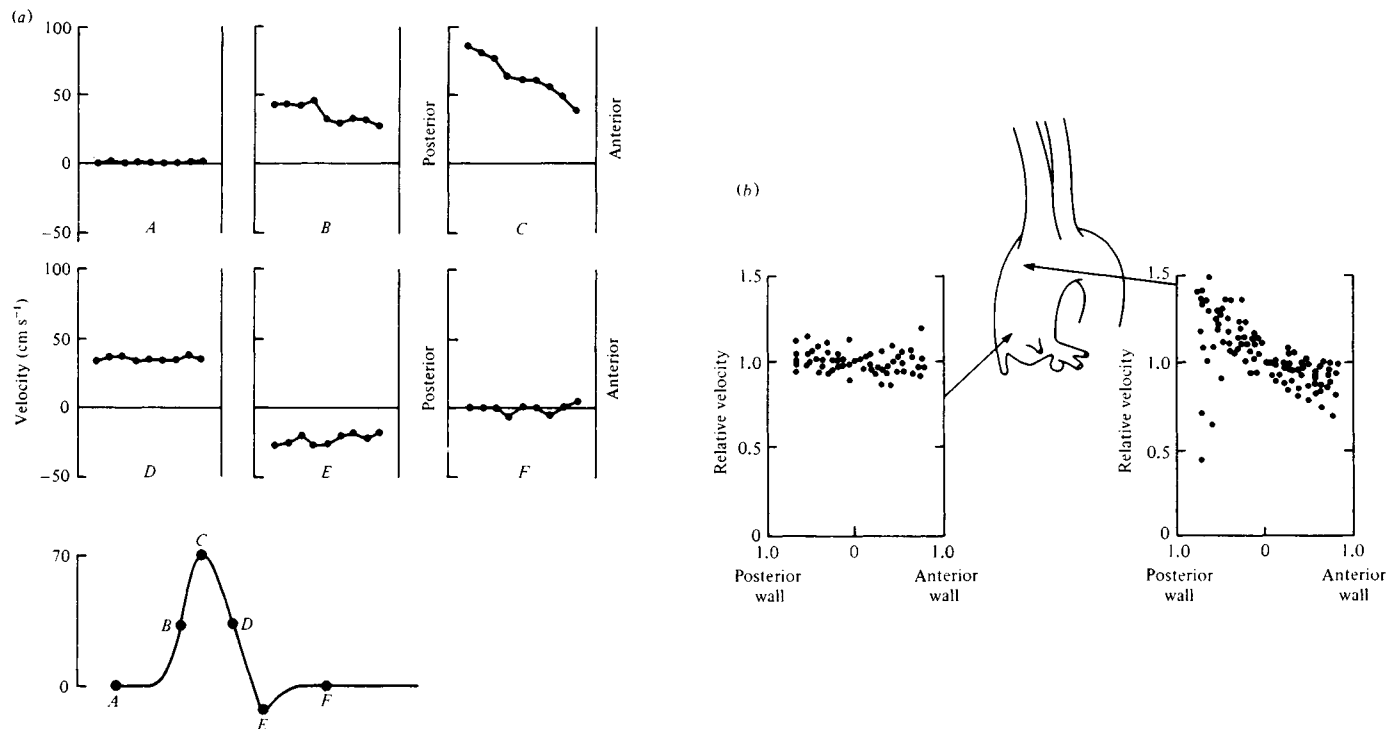


Fig. 1.22. (a) Instantaneous velocity profiles at six different times during the cardiac cycle in the ascending aorta of the dog. The lower figure shows (schematically) the velocity waveform, with the six times marked on it. (b) Velocity profiles at peak systolic velocity across two diameters in the ascending aorta of the dog (velocities scaled with respect to centre-line velocity; radial positions scaled with respect to vessel radius). The profiles at both sites are from several dogs, and were measured in the plane of curvature of the aortic arch. (After Caro *et al.*, 1978.)

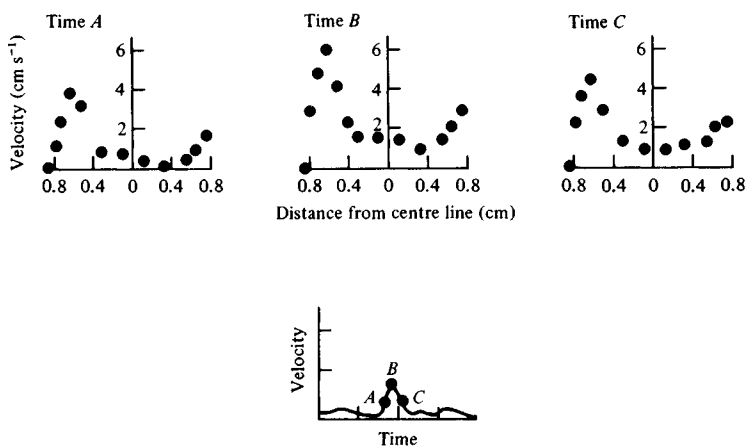


Fig. 1.23. Velocity profiles in the terminal aorta of a horse at various times during the cardiac cycle as indicated; measurements are in the plane of the aortic trifurcation. (After Nerem *et al.*, 1974a.)

Wood). These profiles were measured in the principal plane of curvature of the arch. Profiles have also been measured in a perpendicular plane (Clark & Schultz, 1973) and also show a skewing, towards the left wall. These skews are presumably associated with the geometry of the aorta, i.e. the curvature of the arch, the branches off it and possible misalignment between the ventricular outflow tract and the ascending aorta itself. Furthermore, in diastole, when the average blood velocity has fallen to zero, measurements show a skewed profile immediately downstream of the aortic valve; this may be related to the flow into the coronary arteries, but may also be influenced by disturbances generated during systole. Part of the purpose of chapters 3 to 5 is to explain the observed velocity profiles.

Profiles in the descending aorta remain remarkably flat throughout systole, with a slight skew towards the right wall, but with little apparent influence of the large branches upstream. The profile tends to become rounder with distance from the heart, as indicated by the mean profiles of fig. 1.21.

Schultz *et al.* (1969) reported rather distorted aortic and pulmonary artery velocity profiles in human patients with mitral, aortic or pulmonary valve disease.

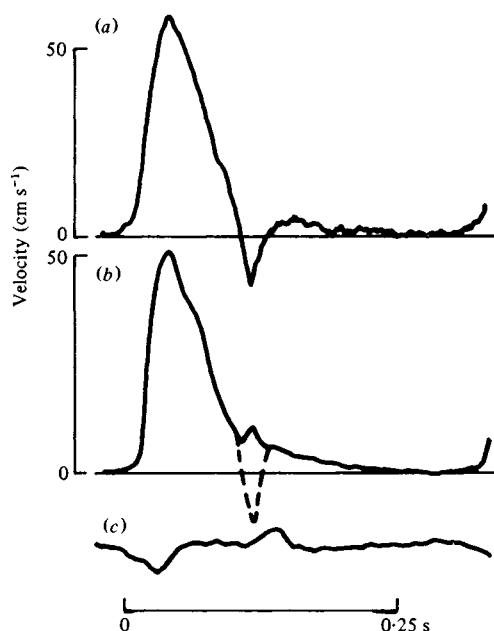


Fig. 1.24. Simultaneous aortic velocity measurements with (a) an electromagnetic flow cuff and (b) a hot-film anemometer located on the vessel centre line. The signal from a second hot-film, (c), indicates when reversal occurs. (After Clark & Schultz, 1973.)

Similar aortic velocity profiles were obtained in the horse (Nerem *et al.*, 1974a). In this animal, however, it is possible to make measurements in the terminal part of the abdominal aorta, distal to the mesenteric and renal branches, as well as in the external iliac and mesenteric arteries themselves. These measurements reflect the complexity of the local geometry, with marked skews and asymmetries. One striking feature is that just before the iliac bifurcation, peak aortic velocities are off the centre of the tube (fig. 1.23), while in the iliac artery the profile is rounded and approximately symmetric.

Finally, some profiles have been measured in horse coronary arteries (Nerem *et al.*, 1974a). Profiles in the left circumflex artery are shown in fig. 1.19, measured in a plane perpendicular to the plane of the common coronary artery bifurcation, which as we have already seen lies on a curved surface. There is a marked skew

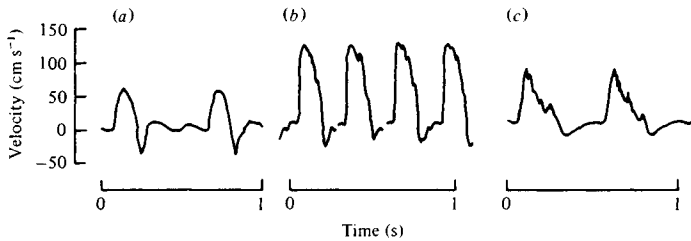


Fig. 1.25. Velocity waveforms recorded in the descending thoracic aorta of dogs: (a) undisturbed, (b) disturbed, (c) highly disturbed. (After Nerem *et al.*, 1972.)

towards the outside of this curve at all stages in the cycle, and this skew is also observed in the left anterior descending artery.

We should note that the presence of relatively flat velocity profiles in most large arteries means that measurements made by a probe only roughly positioned in the centre of the tube (e.g. on a catheter) will be representative of the centre-line velocity, and that the centre-line velocity is close to the average velocity. Fig. 1.24 shows the correspondence between the waveforms of centre-line velocity and of average velocity in the ascending aorta. In regions of complicated geometry, of course, such a correspondence cannot be assumed (cf. fig. 1.23).

1.2.5 *Disturbed or turbulent flow*

Most velocity measurements in the arteries of anaesthetised normal dogs show a smooth variation with time which suggests that random disturbances are absent and that the flow is laminar. Occasionally, however, high-frequency disturbances are noted in the aorta, occurring just after peak forward velocity and either dying out rapidly or persisting until the blood comes virtually to rest in diastole (fig. 1.25). Fourier analysis of the disturbed waveforms shows that the fluctuations cover a wide and continuous frequency spectrum from at least 500 Hz (above which the amplitude is too small for accurate measurement) down to below 25 Hz, where they become indistinguishable from the high-frequency components of the underlying waveform (Nerem & Seed, 1972). The randomness and non-reproducibility from beat to beat of these fluctuations indicate that the disturbances can correctly be referred to as turbulence, although the frequency spectrum is, of course, not the same

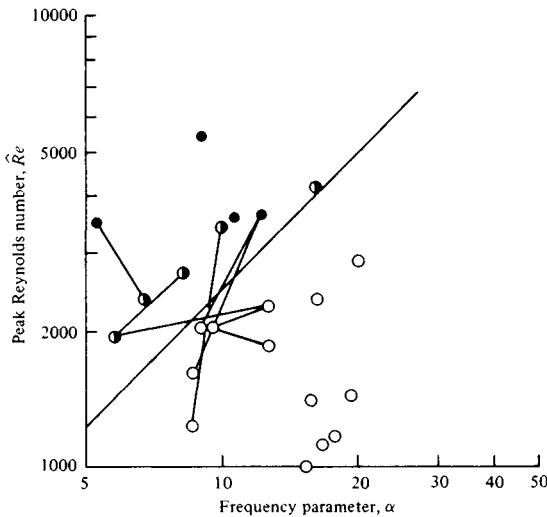


Fig. 1.26. Peak Reynolds number, \hat{Re} , and frequency parameter, α , for the descending thoracic aorta of dogs: open circles, undisturbed flow; half-filled circles, disturbed flow; filled circles, highly disturbed flow; continuous line, (1.9). Points joined together are for the same dog in different physiological states. (After Nerem *et al.*, 1972.)

as that of steady, fully developed pipe flow turbulence; Parker (1977) has analysed the spectrum using a sophisticated ensemble-averaging technique.

By using drugs to vary the heart-rate and cardiac output of their experimental animals, Nerem & Seed (1972) showed that an initially laminar flow could be made to become turbulent. Furthermore, the borderline between laminar and turbulent flow occurred for values of frequency and flow-rate that are close to those of unanaesthetised animals. This can be seen from fig. 1.26, in which the axes are peak Reynolds number, \hat{Re} , and frequency parameter, α ($=\frac{1}{2}d(2\pi f/\nu)^{1/2}$, where d is the diameter of the aorta, f is the heart-rate and ν is the kinematic viscosity of blood). The line

$$\hat{Re} = 250\alpha \quad (1.9)$$

roughly separates the turbulent dogs from the laminar. It is clear that normal dogs may be on either side of this line, which no doubt explains the controversy that has grown up between those who assert that turbulence is not normally present and those who assert

that it is. A simple scaling analysis of the whole animal kingdom, using the plentiful data on heart-rate and cardiac output quoted by Stahl (1967), suggests that \dot{V}_e is proportional to $\alpha^{2.3}$ as body size varies, and that for resting animals this line (on a log-log plot) crosses the line describing (1.9) at a point corresponding to an animal mass of about 25 kg (Pedley, 1978). Roughly speaking, therefore, animals larger than dogs may be expected normally to have turbulent aortic flow and smaller animals may be expected not to. Exercise would make turbulence more likely. Certainly the flow in a horse's aorta is normally turbulent (Nerem *et al.*, 1974a), and measurements by W. A. Seed (personal communication) indicate that man, too, normally has turbulent flow in the aorta. A wider range of experiments would be of great interest. As far as this book is concerned, however, the main interest lies in the origin of the turbulence. Is it a local flow instability, or does it represent the convection to the measuring site of disturbances already present in the ventricle? This question is addressed in § 5.3.

Seed's observations in man conflict with the conventional clinical view that (a) 'aortic murmurs' heard through a stethoscope reflect the presence of turbulence, and (b) murmurs are not heard in normal man, but are primarily heard in conditions of aortic valve stenosis, when the valve cannot open properly and a turbulent jet is ejected each beat. Therefore (c) there is normally no turbulence. One cannot doubt the observations (a) and (b), but only the logic leading to (c). It is quite possible that the vigorous disturbances in a turbulent jet are audible at the chest wall while those in the transitorily disturbed normal aortic flow are not: Seed also reports that faint murmurs are heard through a stethoscope placed on the surface of a normal artery in which the flow is turbulent, but not through one placed on the chest. If stethoscopes of greater sensitivity could be designed, then it might be possible to hear murmurs in normal man.

Apart from its possible diagnostic significance, the presence of turbulence in an artery is known to have an important effect on the material of which the artery wall is comprised. It is an old clinical observation that the walls of a blood vessel often show localised dilatation just downstream of a partial obstruction to the flow, called a stenosis. Roach (1972) has shown that this 'post-stenotic

dilatation' occurs regardless of the origin of the obstruction, as long as it is severe enough to cause turbulence in the downstream flow (and not so severe that the blood flow-rate is cut down to a laminar trickle). Roach also showed that by exposing segments of artery to small-amplitude oscillatory disturbances, then if the disturbance frequency was in the range 25–500 Hz, the wall became significantly more distensible (the higher frequencies having a relatively greater effect on older arteries). This is the range of frequencies present in the turbulent jet downstream of a stenosis over the physiological range of Reynolds numbers, and the conclusion that post-stenotic dilatation is a reflection of such an increased distensibility is inescapable. One is immediately tempted to ask what might be the effect of intermittent turbulence in the aorta, assuming that it normally does occur. The human aorta tends to become stiffer with age, while more peripheral arteries tend to become less stiff (Learoyd & Taylor, 1966). The former effect could conceivably be a chronic response to the degenerative action of arterial turbulence, which could not become apparent in the relatively short-term studies of Roach and her colleagues. A comparison of the changes in aortic distensibility brought about with age in large (turbulent) and small (laminar) animals would be of interest.

The fact that turbulence has an important effect on arterial wall structure means that it would be expected also to influence any physiological process that depends on wall structure. In particular, it may have an influence on the permeability of artery walls to various chemicals, and hence, as discussed in the next subsection, on the initial stages of arterial disease.

1.2.6 *Wall shear stress and arterial disease*

It is becoming increasingly accepted that haemodynamic factors play a role in the initiation of atherosclerosis. This belief is based on a number of observations. It has been noted that fatty streaks, thought by many to be the precursors of the true atheromatous plaques that constitute the disease, are distributed preferentially at certain locations on the artery walls (Caro *et al.*, 1971). Particular sites include the outer walls of arterial junctions (and not the flow dividers), the inside walls of curves (e.g. the aortic arch), the carotid

sinus (an outpouching of the carotid artery, not associated with valves), and the abdominal rather than the ascending aorta. Further experiments in which animals (particularly rabbits and dogs) have been fed high-cholesterol diets have indicated that the distribution of the fatty streaks that develop after a few weeks is roughly the reverse of that just described (see, for example, Newman & Zilversmit, 1962; Cornhill & Roach, 1976). These observations have suggested the hypothesis that the patchy distribution of fatty streaks reflects a non-uniformity in the permeability of artery walls to the lipoproteins on which cholesterol is transported in or out. In the cholesterol-fed animals, the concentration of these substances in the blood is higher than that in the wall, and it is suggested that fatty streaks occur in regions of relatively high permeability, where the rate of influx is greater. In normally fed man, on the other hand, the concentration is thought to be higher in the wall than in the blood, so the lipoproteins can escape more readily through high-permeability regions, which are therefore spared from fatty streaking. This conjectured relation between fatty streaking and wall permeability is still rather tenuous, because the forms in which cholesterol enters and leaves the wall and in which it accumulates in the wall are different, and the links between them are not well understood (Porter & Knight, 1973).

Circumstantial support for the above hypothesis comes from experiments performed *in vivo* with marked large molecules, such as Evans Blue dye (bound to albumin in the plasma) or radioactively labelled fibrinogen or lipoprotein (Fry, 1973; Schwartz *et al.*, 1974; Nerem, Mosberg & Schwerin, 1976). After such substances have been circulating in the blood for some time, some of them will have been transported into the vessel walls, the amount accumulating at any site being roughly proportional to the permeability of the wall there. Post-mortem examination shows that the regions of greatest accumulation, and thus of greatest permeability, are well correlated with the regions in which fatty streaks develop in cholesterol-fed animals.

Although it is possible that some regions of the wall are more permeable than others for genetic reasons, it is more conventional to suppose that the different regions have been subjected to different external influences, in particular, to different mechanical

stresses exerted by the flowing blood. These consist of the pressure and the wall shear stress. There is evidence (Fry, 1973) that an elevated mean pressure enhances wall permeability to large molecules if it results in a marked stretching of the endothelial cell layer (but not otherwise, ruling out pressure-driven filtration as the mechanism for mass transfer); indeed, chronic high blood pressure is known to be a predisposing factor in the development of atherosclerosis. However, an elevated mean pressure would be distributed more or less uniformly over the artery walls, and interest has therefore centred on the role of the wall shear stress. This varies both with time throughout the cardiac cycle and with position in the arterial tree, and there is considerable evidence linking it with wall permeability.

Using excised segments of artery, Fry and his colleagues have shown that an elevated steady wall shear stress, τ_w , increases the permeability of the artery wall (Fry, 1973). Indeed, Carew (1971) found a good correlation between permeability and τ_w^2 , while Caro & Nerem (1973) fitted their data to $\tau_w^{0.29}$, and Nerem *et al.* (1976) found $\tau_w^{0.38}$ to be the best fit for steady shears, but reported a stronger dependence on the amplitude of oscillatory shear stresses (with zero mean), especially when this amplitude exceeded about 5 N m^{-2} . They also found an influence of oscillatory *pressure* (at a frequency of 1 Hz), which is consistent with the idea already encountered that fluctuating forces influence artery wall structure (Roach, 1972). Fry (1973) also quotes evidence that turbulence in the flow can enhance wall permeability.

Fry (1968) has shown further that if the shear stress is maintained for a short time at the (unphysiologically) high level of 40 N m^{-2} or more, then the endothelial surface is irreversibly damaged, and its permeability greatly enhanced. Fry has suggested that this high-shear damage might be a factor in atherogenesis. However, Caro *et al.* (1971) noted that the regions in which fatty streaks develop are those in which the wall shear stress would be expected to be low if the flow in the arteries were steady. This is consistent with the hypothesis that fatty streaks develop in regions of low permeability, and has led to the further hypothesis that fatty streaks and early atheromatous plaques develop preferentially in regions of low wall shear.

Before this hypothesis can be established, several aspects of the process must be more fully understood. These include (i) the link between wall permeability to large molecules and atheroma; (ii) the mechanism by which such large molecules are transported across the endothelium (probably 'pinocytosis' – see Weinbaum & Caro (1976) for a convincing theoretical analysis of the process); (iii) the way in which the wall shear stress influences this mechanism; and (iv) the actual distribution of wall shear stress in the arteries. There is scarcely even a hypothesis to explain (iii), although the wall shear is known to affect the endothelial cell structure, because the cell nuclei are found to align themselves with the direction of the prevailing shear (Flaherty *et al.*, 1972*b*). Caro *et al.* (1971) originally suggested that the rate-controlling step in the transport process was the transfer across a diffusion boundary layer in the blood, and, in a long footnote to that paper, Lighthill rightly argued that the unsteady components of shear stress could have no influence on this. The important haemodynamic factor was therefore thought to be the *mean* wall shear stress. However, Caro & Nerem (1973) have since shown that the diffusion boundary layer cannot be the rate-controlling step, and the reasons for restricting attention to the mean shear stress are no longer valid. The importance of the unsteady components will depend crucially on the time-scale of the events involved in the mass-transfer process, and very little is known of these. Therefore, in pursuing (iv) above, it is important to determine the distribution of both the mean and the fluctuating components of shear stress in large arteries. One must be able to determine the shear-stress variations over a very small length-scale, for, as Cornhill & Roach (1976) have shown, the distribution of fatty streaking round the entrances to the tiny intercostal arteries (fig. 1.3) in cholesterol-fed rabbits is markedly and reproducibly non-uniform, being greatest on the downstream lip. They also noticed a marked non-uniformity from one pair of intercostals to the next, possibly reflecting the development of the flow as it straightens out after the aortic arch, or possibly being a consequence of the distortion caused to the aortic flow by the removal of a little blood into the upstream intercostals (see § 5.2).

It has not yet proved possible to measure unsteady wall shear accurately either *in vivo* or in rigid casts of arteries. This is because

(a) the velocity gradient varies rapidly across a thin boundary layer (less than 2 mm thick) near the arterial wall, so any probe must be accurately embedded in the wall; any protuberance can significantly affect the local distribution of shear stress (Lutz *et al.*, 1977); (b) the frequency response of a shear-stress probe must be much better than that of a velocity probe (see § 3.1); and (c) a hot-film shear-stress probe (the only device that has so far been seriously suggested) rectifies the signal, and therefore cannot be accurate during shear reversal (see § 3.1 and the appendix). It is therefore necessary to study arterial wall shear stress theoretically. Part of chapter 2 and much of chapters 3 to 5 are devoted to this end.

For more biochemical details concerning fatty streaks and atherosclerosis, see Porter & Knight (1973) and Lighthill (1975, chapter 13).

1.2.7 *Korotkoff sounds*

This section should not end without mention of a fascinating problem that has intrigued both clinical physiologists and fluid dynamicists for many years, and for which there is still no completely satisfying explanation. This is the phenomenon of Korotkoff sounds, which are used by clinicians to measure systolic and diastolic arterial blood pressure. A cuff containing an inflatable bag is wrapped round the upper arm, and the bag is inflated to pressures well above the systolic pressure, so that the brachial artery is completely closed off. A stethoscope bell is placed over the artery peripherally, and nothing can be heard through it. Then the cuff pressure is gradually reduced, and when it falls below a certain value a characteristic sharp tapping sound is heard each beat. As the cuff is further deflated, this sound becomes louder and is often accompanied by a brief murmur reminiscent of that associated with aortic valve stenosis. Subsequently the sound becomes noticeably muffled, and finally it disappears altogether. The cuff pressure at which the sounds first appear is usually taken to be systolic pressure, and that at which they are muffled is taken to be diastolic pressure; however, simultaneous, independent, direct measurements suggest that these values can be in error by up to 25% unless the cuff length is at least 1.6 times the arm diameter (see Anliker & Raman, 1966; and Steinfeld *et al.* 1974). Correct interpretation of the pressures

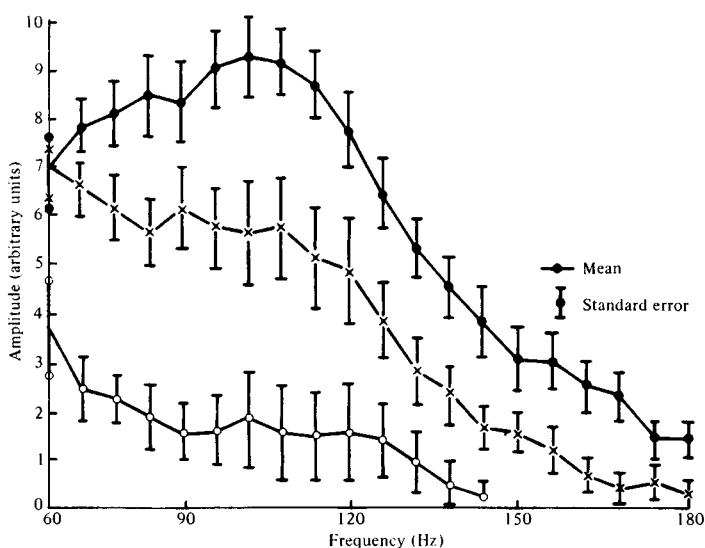


Fig. 1.27. Graph of amplitude against frequency for the high-frequency components of Korotkoff sound: filled circles, sound preceding muffling; crosses, muffled sound; open circles, sound following muffling (background). (After McCutcheon *et al.*, 1967.)

measured in this way will be impossible until there is full understanding of the mechanism by which Korotkoff sounds are produced.

A thorough experimental investigation of the phenomenon was carried out by McCutcheon & Rushmer (1967). They performed a Fourier analysis of the sounds heard before, during and after muffling, showing that it was the frequency components between 60 and 180 Hz that are diminished when muffling occurs (fig. 1.27). By observing the passage through the occluded artery of radio-opaque dyes, these authors were able to show that when the first sound was heard (at a cuff pressure just *below* systolic), a narrow jet could briefly be seen emerging into the stagnant blood downstream of the cuff. The jet soon broke up into turbulence. Observations on casts, made by injecting substances into the arteries of a limb at arterial pressure, while the limb was compressed by a cuff, showed that the cross-sections of the arteries in this situation were non-circular, with smaller area and circumference than usual, which recalls the

behaviour of excised veins under compression. Chapter 6 is devoted to the mechanics of flow through flexible tubes under compression, and includes a description of both model experiments and the theories designed to elucidate them. A discussion of some of the mechanisms put forward to explain Korotkoff sounds is included.

1.3 Fluid mechanics of the left ventricle

In this section we examine some of the fluid mechanical phenomena that accompany the filling and emptying of the left ventricle, as a prelude to the analysis of the arterial system, which occupies the next four chapters. We discuss first the mitral valve, then the aortic valve and finally the overall pressure–flow–rate relations of left ventricular ejection.

1.3.1 *The mitral valve*

The mitral valve is set off the axis of the left ventricle (fig. 1.1) and the jet of fluid that enters through it as the ventricle fills is not symmetrical. Model experiments by Bellhouse (1972) showed that when the jet hit the far wall of the ventricle, it curved round and generated what he described as an asymmetrical vortex ring, with a much more extensive vortex in the outflow tract beneath the aortic valve than on the opposite (posterior) side. This confirms the observations of Taylor & Wade (1970) who took cine-angiographic pictures of flow patterns in the left ventricle *in vivo*. Bellhouse (1972) also showed, in experiments with both life-sized and very large model ventricles (in the latter only a very weak vortex developed), that when ventricular contraction begins, the presence of the vortex helps the mitral valve to close before significant backflow develops. He also showed that in both models, even when operated at the rather low frequency of 0.5 Hz, the cross-sectional area of the aperture began to decrease well before the forward velocity into the ventricle reached its maximum, i.e. while the fluid was still being accelerated forwards.

A simple model of the initiation of mitral valve closure can be developed if we ignore the asymmetry of the jet and the vortex, and model the ventricle as an axisymmetric chamber with the mitral valve on the axis of symmetry (fig. 1.28). Suppose the cusps to form

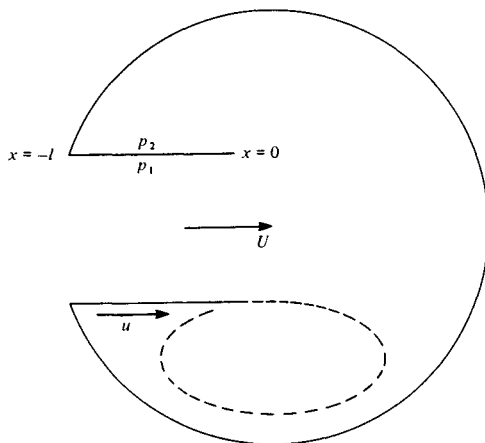


Fig. 1.28. Model for mitral valve closure. The left ventricle is taken to be spherical, and the valve cusps are assumed to form a cylindrical inflow tube. Dotted curve represents the separated vortex sheet. For explanation of symbols, see text.

a parallel-sided orifice when fully open, and suppose that the inflow forms a parallel stream of velocity $U(t)$. If a typical radius of the ventricle is a , then the viscous diffusion time is a^2/ν (ν is the kinematic viscosity of blood) which in man is over half a minute, much greater than the 1 s which is the duration of the cardiac cycle. Therefore the effects of viscosity will be small except in thin boundary layers on the ventricular walls, and in the separation of the stream from the edge of the cusp to form a vortex sheet, which will begin to roll up as indicated in the lower half of fig. 1.28. Apart from this vortex sheet, we assume the flow to be irrotational. The valve will begin to close when the average pressure on the outside of the cusp exceeds that on the inside. These pressures can be estimated from the unsteady form of Bernoulli's equation. On the inside of the cusp, of length l , the longitudinal velocity is U , and the velocity potential ϕ can be written Ux ($x = 0$ at the cusp tip, as shown in fig. 1.28). Thus the pressure, p_1 , is given by

$$p_1/\rho + \dot{U}x + \frac{1}{2}U^2 = p_0/\rho + \frac{1}{2}U^2,$$

where p_0 is the pressure at $x = 0$. The average pressure is then

$$\frac{1}{l} \int_{-l}^0 p_1 dx = p_0 + \frac{1}{2}\rho l \dot{U}. \quad (1.10)$$

On the outside of the cusp, the velocity, u , will vary from zero at the stagnation point at $x = -l$ to a value that may reach U at $x = 0$ when the vortex is strong. As a rough approximation let us take

$$u = U(1 + x/l) \quad \text{and} \quad \phi = U(x + x^2/2l). \quad (1.11)$$

Substitution into Bernoulli's equation then gives the average pressure on the outside to be

$$\frac{1}{l} \int_{-l}^0 p_2 \, dx = p_0 + \frac{1}{3}\rho U^2 + \frac{1}{3}\rho l \dot{U}. \quad (1.12)$$

Thus the difference in the average pressures, from outside to inside, is

$$\frac{1}{3}\rho(U^2 - \frac{1}{2}l\dot{U}). \quad (1.13)$$

This is negative only when $\dot{U} > 0$ and U^2 is not too great; it changes sign before $\dot{U} = 0$. In one of his examples, Bellhouse took

$$U \approx U_0(1 - \cos 2\pi ft),$$

where $U_0 = 0.6 \text{ m s}^{-1}$, $f = 0.83 \text{ Hz}$. The cusp length in his model was 2.8 cm. Change of sign of the quantity (1.13) is then predicted to occur at $t = 0.15 \text{ s}$. In fact, Bellhouse observed it to occur in his life-sized ventricle at $t \approx 0.33 \text{ s}$ (his fig. 12) and presumably our prediction is an underestimate because the vortex does not induce such a vigorous motion on the outside of both cusps as assumed in (1.11). If we neglect the vortex altogether, and suppose the outside pressure to be uniform at $p = p_0$, then (1.13) would be replaced by $-\frac{1}{2}\rho l \dot{U}$, which changes sign at peak forward flow when $\dot{U} = 0$, i.e. at $t = 0.60 \text{ s}$. In Bellhouse's large-ventricle model, where only a very weak vortex is developed, the valve begins to close at $t = 0.5 \text{ s}$, which is consistent with the above ideas.

A more accurate theoretical model of mitral valve behaviour would require specification of the flow while the valve was opening and closing as well as while the cusps were parallel. It would also involve calculation of the position of the separated vortex sheet, which could be done by the methods used by aerodynamicists to compute the rolling-up of a vortex sheet off a delta-wing. However, this would all require lengthy numerical computation, and is probably not worth it unless very subtle fluid dynamical factors prove to be important in the design of artificial valves.

1.3.2 *The aortic valve*

Bellhouse & Talbot (1969) and Bellhouse (1969, 1972) have also performed experiments on models of the tricuspid aortic valve, placed across a tube with a sinus downstream of each cusp. Fig. 1.29 shows a cross-section of one sinus when the valve is open. Flow-visualisation studies showed that (a) the valve cusps opened smoothly; (b) when the tip of a cusp passed the sinus ridge *R*, a three-dimensional vortex motion was initiated in the sinus in which flow entered each sinus at the middle of the ridge, curled back along the sinus wall, then along the cusp to flow out into the main stream at the points of attachment of the cusp free margins; (c) the vortex motion and the position of the cusp (projecting slightly into the sinus) remained roughly steady until some time after the maximum velocity in the aorta, then (d) the cusp began to close smoothly, being over 72% closed before the aortic flow reversed; (e) only 2% of the net forward flow leaked back through the valve; and (f) the velocity profile in the aorta just downstream of the valve was at all times flat (this is very important for aortic fluid dynamics). In a model without sinuses, the cusps, when open, touched the wall of the aorta and the valve closed suddenly and unevenly *after* the velocity had reversed its direction, with up to 25% leakback.

These observations show that the sinuses are essential for smooth valve closure. The vortex motions are not themselves vital, however, as indicated by experiments in which they were rather weak but smooth closure still occurred (van Steenhoven & van Dongen, 1979). This is consistent with a theory like the second of those described above for the mitral valve, in which no vortex motion is present, the uniform pressure in the sinus being equal to p_A , the pressure in the aorta at the downstream edge of the cusp. This leads to the prediction that the valve will close from a parallel-sided open position when the aortic flow begins to decelerate ($\dot{U} = 0$). The presence of the vortex is expected to aid valve closure, however, as in the case of the mitral valve. Furthermore, for the cusps to protrude stably into the sinuses, in steady flow or at peak flow, the dynamic pressure of the vortex is required to balance the slight pressure excess on the aortic side of the cusp due to the divergence of the flow there.

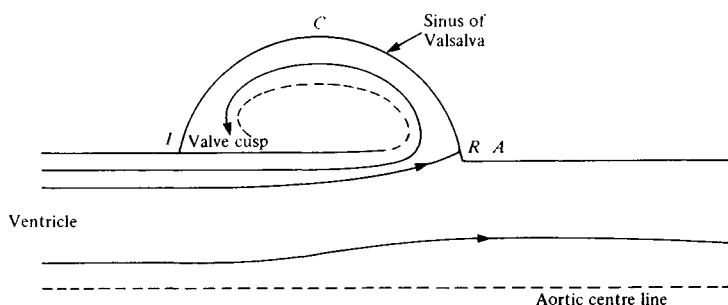


Fig. 1.29. Sketch of the plane of symmetry of a sinus of Valsalva, showing the formation of a vortex in the sinus.

The simplest possible quantitative model of the relations between unsteady pressures and velocities in the aorta and sinuses was given by Bellhouse (1972). Suppose the sinuses to be hemispheres of radius a , and suppose that the upstream and downstream velocity in the aorta (at stations I and A in fig. 1.29) is $U(t)$. Then

$$p_A - p_I = -2\rho a \dot{U}, \quad (1.14)$$

while the pressure on the sinus ridge, R , is stagnation pressure, so

$$p_R - p_A = \frac{1}{2}\rho U^2. \quad (1.15)$$

In the experiments of Bellhouse and Talbot (1969), the maximum velocity in the sinus (at point C) was found to be about $0.9U$; if we assume it to be equal to U , then we also obtain

$$p_R - p_C = \frac{1}{2}\rho U^2, \quad (1.16)$$

so

$$p_C - p_I = -2\rho a \dot{U}, \quad (1.17)$$

while from (1.14) and (1.15),

$$p_R - p_I = \frac{1}{2}\rho U^2 - 2\rho a \dot{U}. \quad (1.18)$$

Bellhouse (1972) reported measurements of U , p_R , p_C , p_I as functions of time, and compared (1.16), (1.17), (1.18) with experiment. The results are shown in fig. 1.30, and agreement is seen to be excellent.

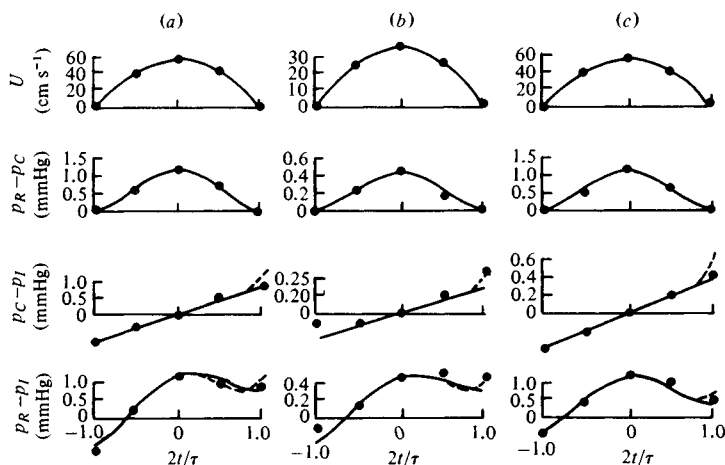


Fig. 1.30. Pressure and velocity measurements for three different ventricular ejections through the model valve. (a) Duration of systole $\tau = 0.575$ s, and peak velocity $u_{\max} = 56.7 \text{ cm s}^{-1}$ (b) $\tau = 0.91$ s, $u_{\max} = 35.0 \text{ cm s}^{-1}$ (c) $\tau = 1.17$ s, $u_{\max} = 56.7 \text{ cm s}^{-1}$. The continuous line represents the simple theory derived in the text; the broken line represents a more complicated theory. (After Bellhouse, 1972.)

In his earlier papers, Bellhouse developed a much more complicated theory than this, involving half a Hill's spherical vortex in each sinus, but the theory was still incomplete since it required an empirically based assumption about the strength of the vortex (such as the assumption that the velocity at C is equal to U). Furthermore, it resulted in negligible improvement in the predictions of pressures in terms of velocity (fig. 1.30). As with the mitral valve, a more complete theory will require the nettle of the rolling-up vortex sheet to be firmly grasped.

1.3.3 The dynamics of left ventricular ejection

In experiments on isolated strips of muscle, the muscle is made to contract against a known load, at a known rate of shortening. In order to apply the results of these experiments to the intact ventricle, therefore, it is important to know the load against which the ventricle contracts. A convenient definition of this 'afterload' is in terms of the average pressure in the left ventricle and the rate of change of its volume. However, a more physiologically useful

definition would be in terms of the pressure and flow-rate at the entrance to the aorta, which are easier to measure, and which are related through the pressure–flow relations of the vessels downstream, i.e. through the ‘input impedance’ of the vascular system (see chapter 2); indeed, Milnor (1975) has suggested using this impedance as a *definition* of ‘afterload’. In this subsection, therefore, we present a simple model relating aortic pressure and flow-rate to ventricular pressure and volume (this model has been previously presented by Pedley & Seed (1977)). The link, involving the momentum of the blood in the ventricle, is not entirely trivial, and gains added importance from the observation by Noble (1968) that the blood momentum can contribute significantly to ventricular ejection. Thus in the latter stages of systole the ventricular muscle may still be shortening when ventricular pressure, and hence the load, is extremely small, a situation that is not normally encountered in papillary muscle experiments.

Any motion of the blood in the ventricle before the aortic valve opens, including both the vortex behind the mitral valve cusps and the motion resulting from the change in shape of the ventricle as it contracts at constant volume (see § 1.1), is ignored. When ventricular pressure p_v exceeds aortic pressure p_a (fig. 1.12) the aortic valve opens and blood is ejected with a flat velocity profile (as discussed in the last subsection and in § 1.2). Let the velocity of the blood being ejected be $U(t)$. This is related to the rate of change of ventricular volume, \dot{V} , by the continuity equation

$$\dot{V} = -AU, \quad (1.19)$$

where A is the cross-sectional area of the aortic valve ring, assumed constant (we ignore the details of aortic valve operation). Hence

$$V(t) = V_0 - A \int_0^t U \, dt, \quad (1.20)$$

where V_0 is the end-diastolic volume of the ventricle, and the valve opens at $t = 0$.

We suppose that the force of contraction of the ventricular muscles can be represented by a single ventricular pressure, p_v , which is the uniform pressure of the fluid in contact with the ventricular wall. This would be strictly true only if the ventricle wall

was a spherical shell, of radius R , with a uniform, isotropic tension T in its walls, so that $p_v = 2T/R$. The use of p_v in the following equations provides an effective definition of it for a non-spherical ventricle. We now apply the integral momentum equation to the blood in the ventricle; this states that the net longitudinal force exerted by p_v against the aortic pressure p_a is balanced by the rate at which momentum is ejected from the ventricle plus the rate of change of momentum of the fluid remaining in the ventricle. That is

$$-\int_S \frac{p}{\rho} (\mathbf{i} \cdot \mathbf{n}) dS = \rho \int_S (\mathbf{u} \cdot \mathbf{n})(\mathbf{u} \cdot \mathbf{i}) dS + \rho \frac{d}{dt} \int_V (\mathbf{u} \cdot \mathbf{i}) dV \quad (1.21)$$

where S is the surface of the control volume, V , comprising the surface of the ventricle, S' , and that of the aortic opening, S_o ; \mathbf{n} is the outward normal to S , and \mathbf{i} is a unit vector in the direction of the axis of the aorta (fig. 1.31).

The left-hand side of (1.21) is equal to

$$(p_v - p_a)A,$$

which defines p_v if the ventricle is not a sphere. The first term on the right-hand side of (1.21) consists of a contribution ρAU^2 from the aperture S_o , assuming that, as observed, the valve ring remains stationary as the ventricle wall moves, and another contribution $-\rho BU^2$ from the ventricle surface S' . In the crudest approximation, BU^2 would be neglected compared with AU^2 , but it can be calculated for any given ventricular shape. In general we write

$$(A - B)U^2 = \beta AU^2, \quad (1.22)$$

and for simplicity take β to be a constant ($= 1$ to first approximation). The case of a spherical ventricle is worked out in detail below.

The second term on the right-hand side of (1.21) is the rate of change of momentum of the fluid in the ventricle. We expect this momentum to be roughly proportional to the volume of the ventricle times the aortic velocity, say

$$\int_V (\mathbf{u} \cdot \mathbf{i}) dV = IVU, \quad (1.23)$$

where I is a number, in general depending on t , but constant if the ventricle and the flow within it remain geometrically similar at all

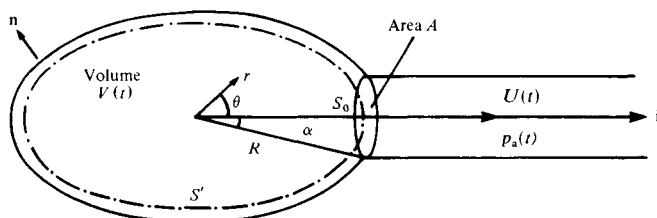


Fig. 1.31. Schematic model of the left ventricle, showing variables and control surface (broken curve) defined in the analysis of ventricular ejection given in the text. (After Pedley & Seed, 1977.)

times. We can calculate I for particular shapes of the ventricle, and again we do so below for the case of the sphere.

Equation (1.21) now reduces to

$$p_v - p_a = \rho \beta U^2 + (\rho/A)(d/dt)(IVU) \\ = \rho(\beta - I)U^2 + \rho(d/dt)(IU)\left(\frac{V_0}{A} - \int_0^t U dt\right). \quad (1.24)$$

This equation may be used in two ways. (i) If the quantities β , I , V_0/A are known, then (1.24) can be used to infer p_v at all times from measurements of aortic pressure, p_a , and velocity, U . This would enable a comparison to be made between the value of p_v measured by the insertion of a catheter into the ventricle and that defined here; both p_a and U could be measured simultaneously with a single aortic catheter. (ii) Alternatively, if the catheter method of measuring p_v is accepted, one could use two catheters to measure U , p_a and p_v simultaneously (as did Noble, 1968), and from these measurements some or all of the unknown quantities in (1.24) can be inferred. In particular, V_0 and A are very hard to measure accurately *in vivo*, complicated analysis of pairs of X-ray photographs, or the invasive use of yet more instruments, being required (Bergel, 1972c). At the time when $\dot{U} = 0$, (1.24) could be used to estimate $\beta - I$ (assuming β and I to be constants), and then the results at two other times could be used to infer I and IV_0/A . Comparison of the experimental results with (1.24) at all other times would constitute a check on the theory leading to that equation. Also the values inferred for β and I could be used to check predictions of those quantities, as made below for a spherical

ventricle. A drawback with this proposed experiment is that the measured values of p_v would already contain some contribution from blood momentum; care would have to be taken to find (empirically) the optimum location of a ventricular catheter.

It is appropriate here to compare the magnitudes of the terms on the right-hand side of (1.24) with measured values of the difference between ventricular and aortic pressure, from the experiments of Noble (1968). According to the theory for a spherical ventricle, presented in the next subsection, the value of $\beta - I$ is predicted to decrease from 0.90 to 0.83 during a contraction in which the ventricular volume falls from 50 cm^3 to 25 cm^3 (representative values for a normal dog), while I is predicted to increase from 0.11 to 0.16. Thus the assumption that these quantities remain constant (at 0.87 and 0.14, say) is a reasonable first approximation. For a peak aortic velocity of 1.2 m s^{-1} (table 1.1), the first term on the right-hand side of (1.24) then takes a maximum value of about 1.3 kN m^{-2} (9.5 mmHg). With a heart-rate of 2 Hz, the maximum positive and negative values of acceleration can be taken to be about $\pm 75 \text{ m s}^{-2}$ (Noble, Trenchard & Guz, 1966). Taking $V_0 = 50 \text{ cm}^3$ and $A = 1.8 \text{ cm}^2$ (corresponding to an aortic diameter of 1.5 cm), the last term in (1.24) is thus predicted to vary in the range $\pm 2.7 \text{ kN m}^{-2}$ ($\pm 20 \text{ mmHg}$). Now in conscious dogs, with heart-rates that varied from 1.5 to 2.0 Hz, Noble (1968) recorded a maximum value of $p_v - p_a$ between 1.6 and 2.3 kN m^{-2} (12 and 17 mmHg), and a minimum between -0.5 and -1.9 kN m^{-2} (-4 and -14 mmHg). Although a detailed comparison of the predicted and the observed pressure differences as functions of time cannot be made from Noble's data, and although the exact relation between the value of p_v measured by him and that defined here remains somewhat obscure, the experimental values are fairly close to the predictions, and confirm that the present model is a reasonable one. Predictions from a more accurate, spheroidal model of the ventricle will clearly be useful.

We may note that, although the values quoted above for the difference between ventricular and aortic pressure are small compared with mean aortic pressure (13.3 kN m^{-2}), the larger values amount to about a half of the variation of aortic pressure which takes place each beat (the 'pulse pressure'). Thus the time

variation of canine ventricular pressure is not accurately represented by that of aortic pressure. (Similar results are predicted for man.) Furthermore, in a subject in which the peak aortic velocity is as high as 2 m s^{-1} (as may happen either with a stenosed or an incompetent aortic valve), the difference between ventricular and aortic pressure is predicted to be even greater and indeed to be a significant proportion of mean aortic pressure.

Another way of looking at ventricular dynamics is by way of the energy equation, which may be written

$$\frac{\partial}{\partial t} \int_V \frac{1}{2} \rho q^2 dV + \int_{S'} (\mathbf{u} \cdot \mathbf{n}) (p + \frac{1}{2} \rho q^2) dS = -UA(p_a + \frac{1}{2} \rho U^2), \quad (1.25)$$

where $q = |\mathbf{u}|$, the fluid speed. The right-hand side is a surface integral, like the second term on the left-hand side, evaluated over the surface S_0 spanning the entrance to the aorta. This integral represents the rate at which energy is delivered to the aorta. If (1.25) is integrated with respect to time, from the time of valve opening to the time of valve closure, then we see that the work done by the ventricular muscle (the left-hand side) equals

$$-\int (p_a + \frac{1}{2} \rho U^2) dV$$

and this is approximately equal to $-\int p_a dV$ if the dynamic pressure $\frac{1}{2} \rho U^2$ is neglected. This 'stroke work' has for many years been taken as an index of cardiac contractility, despite the fact that it depends strongly on aortic pressure, which is determined as much by peripheral conditions as by the direct action of the ventricle (Blinks & Jewell, 1972). Skalak (1972) and McDonald (1974) give full accounts of the energetics of the whole circulatory system. It is clear that for given peripheral conditions the energy equation is a simple and adequate representation of overall ventricular behaviour (at least as long as the kinetic energy terms can be neglected), but I believe that the momentum equation is more suitable for examining ventricular dynamics throughout ejection.

1.3.4 *The case of a spherical ventricle*

Here we give more precise calculations of the quantities β and I (see (1.22) and (1.23)) for the case where the ventricular surface S'

is part of a sphere S of radius R . The exit control surface S_0 is taken to be the completion of the sphere S . We take the valve ring to remain fixed while the ventricular wall moves towards it during contraction. We further take the valve ring to be a circle of radius $R \sin \alpha$, which normally remains approximately constant while the ventricle contracts, so α will increase as R decreases. We assume that viscous effects are negligible, since the viscous diffusion time is large compared with the period of the heart beat. Thus the motion will be irrotational as well as axisymmetric, and can be described by a velocity potential ϕ . This is the solution in $r < R$ of

$$\nabla^2 \phi = 0; \quad \partial \phi / \partial r = f(\cos \theta) \quad \text{on } r = R$$

where

$$\begin{aligned} f(\cos \theta) &= U \cos \theta \quad 0 \leq \theta \leq \alpha \\ &= \dot{R}(1 - \cos \theta / \cos \alpha) \quad \alpha < \theta \leq \pi. \end{aligned} \quad (1.26)$$

(see fig. 1.31). The function $f(\cos \theta)$ is the normal velocity on the boundary of the sphere; its value in $\alpha < \theta \leq \pi$ derives from the facts that the velocity of a point of the ventricle wall is

$$\dot{R}\mathbf{n} - (d/dt)(R \cos \alpha)\mathbf{i}$$

and that $R \sin \alpha$ is constant. The solution for ϕ can be expressed in terms of Legendre polynomials as

$$\phi = U \sum_{n=0}^{\infty} \alpha_n \frac{r^n}{R^{n-1}} P_n(\cos \theta);$$

the boundary conditions imply

$$U\alpha_n = \frac{2n+1}{2n} \int_{-1}^1 P_n(\mu) f(\mu) d\mu. \quad (1.27)$$

Now the linear momentum per unit mass, from (1.23), is equal to

$$\begin{aligned} \mathbf{i} \cdot \int_V \nabla \phi dV &= \int_S \phi \cos \theta dS \\ &= U \int_{-1}^1 \sum_{n=0}^{\infty} R \alpha_n P_n(\mu) \cdot \mu \cdot 2\pi R^2 d\mu \\ &= \frac{4}{3} \pi R^3 U \alpha_1. \end{aligned}$$

Hence $I = \alpha_1$, and this can be calculated from (1.27), using (1.26)

and the facts that

$$AU = -4\pi R^2 \dot{R} \quad \text{and} \quad A = \pi R^2 \sin^2 \alpha. \quad (1.28)$$

The result is

$$I = [(1-c)/16c](2 + 13c + 11c^2 + 7c^3 - c^4)$$

where $c = \cos \alpha$; this is tabulated for various values of α in table 1.3. It can be seen that the assumption of constant I as the ventricle contracts will be very approximate if α varies sensibly.

Table 1.3. *Hydrodynamic constants for a spherical left ventricle at different values of the angle subtended by the aortic opening*

α	$\cos \alpha$	$I = \alpha_1$	β_1	β_2	β	$\beta - I$
18.2°	0.95	0.097	0.93	0.098	1.03	0.93
25.8°	0.90	0.19	0.87	0.12	0.99	0.80
31.8°	0.85	0.27	0.81	0.13	0.94	0.67
36.9°	0.80	0.35	0.74	0.14	0.88	0.53
45.6°	0.70	0.50	0.62	0.13	0.75	0.25
60°	0.50	0.75	0.36	0.11	0.47	-0.28
78.5°	0.20	1.27	-0.69	0.028	-0.66	-1.93
<i>Dog</i>						
20.0°	0.94	0.12	0.92	0.10	1.02	0.90
24.5°	0.91	0.17	0.88	0.12	1.00	0.83
<i>Man</i>						
23.1°	0.92	0.15	0.90	0.11	1.01	0.86
29.5°	0.87	0.24	0.83	0.13	0.96	0.72

The quantity β is derived from the first integral on the right-hand side of (1.21), in which $(\mathbf{u} \cdot \mathbf{n})$ is the same as $f(\cos \theta)$ while

$$\mathbf{u} \cdot \mathbf{i} = f(\cos \theta) \cos \theta - (1/R)(\partial \phi / \partial \theta) \sin \theta.$$

Hence

$$\beta AU^2 = 2\pi R^2 \int_{-1}^1 f^2(\mu) \mu \, d\mu + 2\pi R \int_{-1}^1 f(\mu) \frac{\partial \phi}{\partial \mu} (1 - \mu^2) \, d\mu;$$

we rewrite the first term as $\beta_1 AU^2$ and the second as $\beta_2 AU^2$. The

first integral is easy to evaluate, and yields

$$\beta_1 = (1/96c^2)(-c^6 + 55c^4 + 8c^3 + 45c^2 - 8c - 3),$$

which is also tabulated in table 1.3. The second integral, derived from the tangential components of velocity on the spherical surface, must be evaluated from the series solution for ϕ . After some reorganisation, this gives

$$\beta_2 AU^2 = 2\pi R^2 U \sum_{n=1}^{\infty} \alpha_n \int_{-1}^1 f(\mu)(1-\mu^2)P'_n(\mu) d\mu;$$

the integrand can be rewritten using the standard recurrence relations for $P_n(\mu)$, so that

$$\begin{aligned} \beta_2 AU^2 &= 2\pi R^2 U \sum_{n=1}^{\infty} \frac{n(n+1)}{2n+1} \alpha_n \int_{-1}^1 f(\mu)[P_{n-1}(\mu) - P_{n+1}(\mu)] d\mu \\ &= 4\pi R^2 U^2 \sum_{n=2}^{\infty} \frac{(n-1)n\alpha_{n-1}\alpha_n}{4n^2-1} \end{aligned} \quad (1.29)$$

from (1.27), after some manipulation. Thus evaluation of β_2 requires evaluation of the α_n and summation of the above series.

The values of $I (= \alpha_1)$, β_1 , β_2 , β and $\beta - I$ are given for various values of α in table 1.3. It immediately becomes apparent that, if α changes appreciably during ventricular contraction, then so will β (if α is large) and I , and the assumptions of constant β and constant I will be inadmissible. In practice, however, quite considerable changes in ventricular volume can take place without large changes in α . For example, for a dog in which (a) the end-diastolic ventricular volume is 50 cm³, (b) the volume after ejection is 25 cm³, and (c) the diameter of the aortic ring is 1.50 cm, the values of α at the beginning and end of the contraction (assuming a spherical ventricle) are 20.0° and 24.5°. The corresponding values for I and β can be seen from table 1.3 to vary by 42% and 2% respectively over this range of α . Similarly, in a man with an end-diastolic volume of 140 cm³, an end-systolic volume of 70 cm³, and an aortic ring diameter of 2.5 cm, the values of α before and after contraction are 23.1° and 29.5°. The corresponding variations in I and β are then 60% and 5% respectively. Thus the assumption of constant β (and

of constant $\beta - I$) is reasonably good, but that of constant I is not. An improved theory based on a spheroidal model of the ventricle is now under way; the experiments necessary to validate (1.24) and to assess the catheter measurement of ventricular pressure are being performed by Dr. W. A. Seed of the Charing Cross Hospital, London.